Published in final edited form as:

J Immunol. 2018 November 01; 201(9): 2799–2811. doi:10.4049/jimmunol.1800952.

The histone demethylase LSD1 regulates B cell proliferation and plasmablast differentiation[1]

Robert R. Haines, **Benjamin G. Barwick**[1], **Christopher D. Scharer**, **Parimal Majumder**, **Troy D. Randall**[2], and **Jeremy M. Boss**[**]

Department of Microbiology and Immunology, Emory University School of Medicine, Atlanta, GA, USA

[1]Current address: Department of Hematology and Medical Oncology, Emory University School of Medicine, Atlanta, GA, USA

[2]Division of Clinical Immunology and Rheumatology, Department of Medicine, University of Alabama at Birmingham, Birmingham, AL 35294

Abstract

B cells undergo epigenetic remodeling as they differentiate into antibody-secreting cells. LSD1 is a histone demethylase known to decommission active enhancers and cooperate with the antibody-secreting cell master regulatory transcription factor Blimp-1. The contribution of LSD1 to ASC formation is poorly understood. Here we show that LSD1 is necessary for proliferation and differentiation of mouse naïve B cells into plasmablasts. Following lipopolysaccharide inoculation, LSD1-deficient hosts exhibited a two-fold reduction of splenic plasmablasts and serum IgM. LSD1-deficient plasmablasts exhibited derepression and superinduction of genes involved in immune system processes, a subset of these being direct Blimp-1 target repressed genes. Cell cycle genes were globally downregulated without LSD1, which corresponded to a decrease in the proliferative capacity of LSD1-deficient activated B cells. Plasmablasts lacking LSD1 displayed increased histone H3 lysine 4 monomethylation and chromatin accessibility at naïve B cell active enhancers and the binding sites of transcription factors Blimp-1, PU.1, and IRF4 that mapped to LSD1 repressed genes. Together these data show that LSD1 is required for normal *in vivo* plasmablast formation, distinguish LSD1 as a transcriptional rheostat and epigenetic modifier of B cell differentiation, and identify LSD1 as a factor responsible for decommissioning naïve B cell active enhancers.

Introduction

Humoral immunity against pathogens is achieved through the function of antibody-secreting cells (ASC). In response to antigen, the ASC compartment is generated from the differentiation of naive B cells (nB) and is populated by short-lived mitotically active

[**]Address correspondence to: Jeremy M. Boss, Ph.D., jmboss@emory.edu, phone: 404-727-5973.

The authors declare no competing financial interests.

Data Availability

Sequencing data are available through accession GSE114777, (https://www.ncbi.nlm.nih.gov/geo/query/acc.cgi?acc=GSE114777) at the NCBI Gene Expression Omnibus.

plasmablasts (PB) and long-lived non-cycling plasma cells (PC) (1). Depending on the antigen, nB can give rise to a variety of responses, each evolved to efficiently neutralize the target pathogen in an antigen-specific manner (2). nB interactions with T cell-dependent (TD) antigens results in a two-phase response. The first phase, known as the extrafollicular response results in the generation of short-lived PB that secrete mostly IgM (3). The second phase requires the formation of germinal centers that produce PC and memory B cells. nB interactions with T cell-independent (TI) antigens, such as bacterial lipopolysaccharide (LPS), primarily results in the rapid generation of PB through an extrafollicular response (4).

As nB differentiate to ASC, they undergo widespread changes in gene expression mediated by transcription factors such as Blimp-11, XBP-1, IRF4, and PU.1 (1, 5). To support the demand of constant, substantial antibody production, ASC upregulate the expression of genes that function in metabolic processes (6), as well as protein production, modification, and trafficking (7). Transcriptional changes in ASC are accompanied by changes in the epigenome. For example, in response to LPS, global and specific increases in gene expression occur in the newly formed PB that is accompanied by alterations in chromatin accessibility at enhancers (8) and a reciprocal decrease in DNA methylation (9). PB also exhibit alterations in H3K4me2, H3K4me3, H3K9ac, H3K27me3, and chromatin accessibility at Blimp-1 binding sites (10). Blimp-1 recruits the chromatin-remodeling and histone-modifying complexes BAF, NuRD, and PRC2 to regulate its target genes in PB (10). Within the PRC2 complex, the histone methyltransferase EZH2 is critical for PB formation through H3K27me3-linked repression of transcription factor networks (11). However, the degree to which other epigenetic modifying enzymes regulate ASC differentiation and how they influence promoter and enhancer chromatin throughout this process remains poorly understood.

Lysine-specific demethylase 1 (LSD1) is a monoamine oxidase that demethylates H3K4me1, H3K4me2, H3K9me1, and H3K9me2 through an FAD-dependent amine oxidation mechanism (12, 13). The protein structure of LSD1 consists of an enzymatically active amine oxidase-like domain, as well as SWIRM and Tower domains that facilitate protein-protein interactions (14). By interacting with lineage-specific chromatin modifying complexes, LSD1 regulates multiple cellular differentiation pathways, including embryonic stem cell differentiation (15), neurogenesis (16), and hematopoiesis (17). Known complexes in which LSD1 functions as a co-activator or co-repressor include those containing CoREST (18), HDAC1/2 (18), the androgen receptor (12), and the estrogen receptor (19). Importantly, LSD1 is the only histone demethylase proven to decommission enhancers during cellular differentiation by demethylating the active enhancer modification H3K4me1 (15). In the context of plasma cell differentiation, LSD1 has been shown to interact with Blimp-1 (20). The extent to which LSD1 regulates transcriptional and epigenetic changes that occur during B cell differentiation has not been determined.

Here, LSD1 expression was found to specifically increase as PB form during B cell differentiation, indicating a potential role for this protein during the process. Conditional genetic deletion of *Lsd1* in mice was used to examine its function in PB formation. LSD1 was necessary for normal LPS-induced differentiation of nB into $CD138^{+}$ PB. LSD1 repressed genes were involved in immune system processes, including Blimp-1 target genes.

Cellular proliferation was also impaired in LSD1-deficient B cells and this was coupled to reduced expression of cell cycle genes. Mechanistically, LSD1 reduced local chromatin accessibility at naïve B cell active enhancers and PU.1, IRF4, and Blimp-1 target binding sites. Without LSD1, H3K4me1 accumulated at enhancers of LSD1-regulated genes, supporting a role for this epigenetic factor in modulating gene expression. Cumulatively, this study shows that LSD1 is required for normal B cell proliferation and differentiation and functions as a transcriptional rheostat and epigenetic modifier throughout this process.

Materials and Methods

Animal Protocols

Lsd1$^{fl/fl}$*Cd19*$^{Cre/+}$ mice were generated from breeding *Cd19*$^{Cre/+}$ mice (21) (Jackson Labs 006785) with *Lsd1*$^{fl/fl}$ mice received as a gift from Dr. David Katz (previously described (22)). *Lsd1*$^{fl/fl}$*Rosa26*$^{CreERT2/+}$ mice were generated from breeding *Rosa26*$^{CreERT2/+}$ mice (23) (Jackson Labs 008463) with *Lsd1*$^{fl/fl}$ mice. Experiments were performed on mice eight to twelve weeks old. All experiments were approved by the Emory University Institutional Animal Care and Use Committee. Sequences used for PCR genotyping of mice are listed in Supplemental Table 3. For LPS experiments, mice were i.v. injected into the tail vein with 50 μg LPS from *Salmonella minnesota* R595 (Enzo Life Sciences) diluted 1:1 in PBS as previously described (24). Spleens were isolated on day 3 for the analyses presented. For influenza experiments, mice were infected intranasally with 15,000 viral focal units of A/PR8/34 (PR8) influenza virus (25). Mediastinal lymph nodes were isolated on day 7 for the analysis presented.

In some experiments, B cells were adoptively transferred to naïve mice. CD43 (Ly-48) MicroBeads (Miltenyi Biotec 130–097-148) were used to magnetically purify CD43$^-$ splenic B cells from naïve mice according to the manufacturer's instructions. Purified cells were either transferred into μMT host mice (i.v. injected into the tail) or stained with 5 μM CellTrace Violet (CTV, Invitrogen C34557) for twenty minutes at room temperature protected from light. CTV stained cells were washed with five volumes of B cell media (RPMI 1640, 10% heat-inactivated FBS, 0.05 mM 2-βME, 1X non-essential amino acids, 1X Penicillin Streptomycin, 10 mM HEPES, 1 mM sodium pyruvate) and were adoptively transferred into μMT host mice.

Tamoxifen was used to activate Cre-mediated recombination in *Rosa26*$^{CreERT2/+}$ mice. Tamoxifen powder (Sigma T5648) was dissolved in 100% EtOH at a concentration of 40 mg/300 μl. The tamoxifen was solubilized with ten minutes of sonication, then 1 ml of corn oil pre-warmed to 37°C was added per 300 μl EtOH. The solution was sonicated for fifteen additional minutes and then ethanol was evaporated to yield a 40 mg/ml tamoxifen-corn oil solution. Mice received daily 100 μl injections of 40 mg/ml tamoxifen intraperitoneally (IP) for five days. Following five additional days of rest, mice underwent experimental analyses.

Ex Vivo B Cell Differentiation

CD43^{-} splenic B cells purified as above were cultured at a concentration of 0.5×10^6 cells/ml in B cell media with 20 μg/ml LPS (Sigma L2630), 20 ng/ml IL-2 (eBioscience 14–8021), and 5 ng/ml IL-5 (eBioscience 14–8051) as previously described (24).

Flow Cytometry

Cells were resuspended at a concentration of 10^6 cells/100 μl fluorescence-activated cell sorting (FACS) buffer (1X PBS, 2 mM EDTA, 1% BSA). Cells were stained with Fc block (BD Biosciences) for fifteen minutes, stained with antibody-fluorophores for one hour on ice, then washed with ten volumes of FACS buffer. The following antibodies were used: B220-PE-Cy7 (RA3–6B2, Tonbo), CD11b-APC-Cy7 (M1/70, Tonbo), CD45.1-FITC (A20, Tonbo), CD45.2-PerCP-Cy5.5 (104, Tonbo), CD90.2-APC-Cy7 (30-H12, BioLegend), F4/80-APC-Cy7 (BM8, BioLegend), CD138-BV711 (281–2, BD), CD21-APC (B-ly4, BD), CD43-PE (S7, BD), GL7-eFluor660 (GL-7, eBioscience), CD23-eFluor450 (B3B4, eBioscience), IgM-FITC (II/41, eBioscience), Annexin V-APC (kit number 88–8007-72, eBioscience), and Zombie Yellow Fixable Viability Dye (kit number 423104, BioLegend). An LSRII was used for analysis and an ARIAII was used for sorting (BD Biosciences). All flow cytometry data was analyzed with FlowJo version 9.9.5. Preceding all flow cytometry analyses presented is the following gating strategy: 1) lymphocytes (forward scatter [FSC]-area by side scatter [SSC]-area), 2) singlets (FSC-width by FSC-height), 3) singlets (SSC-width by SSC-height), 4) live cells (viability dye^{-}), 5) exclusion of non-B cell lineage cells (Thy1.1^{-}F4/80^{-}CD11b^{-}).

Enzyme-Linked Immunosorbent Assay (ELISA)

Flat-bottom ELISA plates (Sigma M9410–1CS) were coated with goat anti-mouse Ig (Southern Biotechnology 5300–05B). Plates were incubated overnight at 4°C, washed (1X PBS with 0.05% Tween 20), blocked with 1% non-fat dry milk for two hours at room temperature, washed, incubated with diluted serum samples or mouse IgM (Southern Biotechnology 5300–01B) for two hours at room temperature, washed, incubated with 1:1000 diluted HRP-conjugated goat anti-mouse IgM (Southern Biotechnology 1021–05) for two hours at room temperature, and washed. Plates were incubated with TMB ELISA peroxidase substrate (Rockland TMBE-1000) for twenty minutes at room temperature (50 μl/well) to develop a color reaction. 50 μl of 0.2 M sulfuric acid was applied to each well to stop the HRP color reaction. After twenty minutes, optical density at 450 nm (OD_{450}) was collected by a Synergy HT Multi-Mode Microplate Reader (BioTek).

RNA-seq and Data Analysis

For each sample, 50,000 cells were isolated via FACS into 600 μl RLT buffer (Qiagen, Inc.) containing 1% βME. Samples were vortexed for one minute on high to lyse cells, and External RNA Controls Consortium (ERCC) spike-in transcripts (26) were added (5 μl of 1:2000 dilution per sample) to enable downstream mRNA/cell calculations. Total RNA was isolated using a Zymo Quick-RNA MicroPrep Kit (11–328M). 1 μg of RNA per sample was used to create libraries with a KAPA mRNA HyperPrep Kit (KK8581). An Agilent Bioanalyzer was used to quality check each library. Libraries were pooled at an equimolar

ratio and sequenced on a HiSeq 2500 system (Illumina) using 50 base pair paired-end chemistry.

Raw sequencing reads were mapped to the mm9 genome using TopHat2 (27). Gene counts were determined with the Bioconductor package GenomicAlignments (28) using the mm9 transcriptome database. A gene was considered detected if all three samples from a sample group had at least 0.2 mRNA/cell, which was the minimum ERCC transcript/cell concentration to detect at least 90% of that particular transcript across all samples. The Bioconductor package edgeR (29) was used to determine differentially expressed genes based on both relative (false discovery rate (FDR) ≤ 0.05, no fold change cutoff) and absolute changes (FDR ≤ 0.05, no fold change cutoff) in expression as previously described (9). All differentially expressed genes (DEG) determined are listed in Supplemental Table 1. GO analysis was performed with DAVID (30). Preranked Gene Set Enrichment Analysis (31) was performed on all detected transcripts ranked based on the following equation:

$$\text{sign of fold change}\left(-\log_{10}(\text{edgeR P value})\right)$$

Observed/expected (obs/exp) ratios were calculated through permutation testing against gene sets randomly chosen from all detected genes (1,000 permutations per test).

Assay for transposase accessible chromatin (ATAC)-seq and Data Analysis

ATAC-seq (32) was performed using 10,000 FACS-isolated cells that were resuspended in nuclei lysis buffer (10 mM Tris pH 7.4, 10 mM NaCl, 3 mM $MgCl_2$, 0.1% IGEPAL CA-630) and centrifuged at 500 g for 30 minutes. Samples were transposed with 25 μl tagmentation reaction mix (2X Tagmentation Buffer and 1 μl Tagmentation Enzyme from the Illumina Nextera DNA Library Prep Kit) at 37°C for one hour, diluted two-fold in tagmentation clean-up buffer (300 mM NaCl, 100 mM EDTA, 0.6% SDS, 1.6 μg Proteinase-K), and incubated for 30 minutes at 40°C. Size selection with solid phase reversible immobilization (SPRI) beads was used to isolate low-molecular weight transposed DNA, which was amplified with 2X KAPA HiFi HotStart Ready Mix and Nextera indexing primers (Illumina). To enrich for low molecular weight DNA, a second size selection with SPRI beads was performed post-PCR. Libraries were quality checked and sequenced as above.

Raw sequencing reads were mapped to the mm9 genome using Bowtie (33). Peaks were called using MACS2 (34) and annotated using HOMER (35). Data were normalized to reads per peak per million (rppm) as previously described (36). The Bioconductor package edgeR(29) was used to determine differentially accessible regions (DAR). A Benjamini-Hochberg FDR ≤ 0.05 and a log fold change (logFC) ≥ 1 was required for significance. All DAR determined are listed in Supplemental Table 2. Obs/exp ratios were calculated through permutation testing against peaks randomly chosen from all peaks detected with ATAC-seq (1,000 permutations per test). Tissue-specific enhancer data was previously determined (9). For odds ratio (OR) calculations, the reference group was all ATAC-seq peaks detected (71,925) and significance was determined using Fisher's exact test. Motif analysis was

performed with the HOMER program findMotifsGenome.pl using randomly generated genomic sequences as background.

ChIP-seq data analysis

Public datasets were downloaded from GEO. Peaks were called using MACS2 and annotated using HOMER. For H3K4me2 scatter plots, the reads per million (rpm) data from nB and PB were quantile normalized.

qRT-PCR

Per sample, 50,000 cells were sorted via FACS into 600 μl RLT-βME and processed as with RNA-seq. Total RNA was reverse transcribed with SuperScript II reverse transcriptase (Invitrogen 18064014). cDNA was diluted five-fold and qPCR was performed with a CFX96 instrument (BioRad) using SYBR Green incorporation. Gene expression was calculated relative to ERCC transcript #130. Sequences for all primers are listed in Supplemental Table 3. A Student's two-tailed t-test was used to determine statistical significance.

Chromatin Immunoprecipitation (ChIP) assays

For ChIP-seq analyses, public datasets were downloaded from GEO. Peaks were called using MACS2 and annotated using HOMER. For H3K4me2 scatter plots, the rpm data from nB and PB were quantile normalized.

For ChIP-qPCR assays, PB and nB for ChIP were collected from LPS-inoculated and naïve mice, respectively. PB were collected by staining splenocytes with CD138-APC (281–2, BioLegend), then purifying with anti-APC MicroBeads (Miltenyi Biotec 130–090-855). $CD43^{-}$ splenic B cells were purified as above and represent nB. ChIP-qPCR assays were performed as described previously (37–39). Briefly, cells were cross-linked in 1% formaldehyde for ten minutes, and chromatin lysate was prepared and sonicated to generate fragments averaging 500 bp in length. For immunoprecipitations, anti-H3K4me1 (MilliporeSigma 07–436) and anti-IgG (MilliporeSigma 12–370) antibody was used. Protein G beads (Invitrogen 10004D) were used to isolate the chromatin-antibody complexes. After washing, the immunoprecipitated chromatin was eluted in 1% SDS and incubated overnight at 65°C to reverse the formaldehyde-induced crosslinks. The DNA was purified and used as a template in real-time PCR. DNA was quantitated by qPCR using a 5-point genomic DNA standard curve and an I-cycler (BioRad). qPCR mixtures contained 5% dimethyl sulfoxide (DMSO), 1 SYBR green (Bio Whittaker Molecular Applications), 0.04% gelatin, 0.3% Tween 20, 50 mM KCl, 20 mM Tris (pH 8.3), 3 mM $MgCl_2$, 0.2 mM deoxynucleoside triphosphate (dNTP), and 100 nM of each primer. Sequences for all primers are listed in Supplemental Table 3. All experiments were performed for a total of six times from independent preparations of chromatin. The data were averaged and plotted with respect to the input chromatin. A Student's two-tailed t-test was used to determine statistical significance.

Results

H3K4 methylation is remodeled during B cell differentiation

H3K4me2 is broadly associated with enhancers, promoters, and gene bodies and is correlated with transcription in multiple cell types and organisms, including mammalian immune system cells (15). The dynamics of H3K4 methylation in B cell differentiation was examined by comparing the changes in H3K4me2 enrichment between nB (40) and PB derived from an *ex vivo* LPS differentiation model (10) (Fig. 1A). The comparison revealed that in PB, 6,209 genomic regions gained (red, I) while 6,592 regions lost H3K4me2 (blue, II), indicating that H3K4me2 is remodeled throughout B cell differentiation. To examine the relationship between the changes in H3K4me2 and gene expression, regions that gained and lost H3K4me2 were mapped to within 20 kb of all differentially expressed genes (DEG) between nB vs. LPS-induced PB defined previously (9). Comparison of the $\log_2$ fold changes of the DEG mapping to regions that gained or lost H3K4me2 modifications in PB indicated that changes in gene expression were positively associated with changes in H3K4me2 (Fig. 1B) and suggests that this mark is remodeled and correlated with transcription during PB formation.

To understand how H3K4me2 was remodeled, the expression of known H3K4 demethylases was analyzed from data derived from discrete B cell divisions during differentiation to PB *in vivo* in response to LPS (9). *Kdm1a* and *Kdm5c*, encoding the H3K4 histone demethylases LSD1 and JARID1C, respectively, were progressively upregulated throughout the differentiation process (Fig. 1C). Other members of the family were not induced or expressed at appreciable levels in dividing B cells or PB. LSD1 was chosen for further investigation due to its known interaction with key ASC regulatory transcription factor Blimp-1 (20) and for its ability to decommission enhancers by catalyzing H3K4me2/me1 to an unmethylated H3K4 ground state (15).

LSD1 is required for normal plasmablast formation

To examine the role of LSD1 during B cell differentiation, a floxed *Lsd1* mutant allele (22) was bred onto the $Cd19^{Cre/+}$ background (21) to generate a B cell specific conditional knockout (CKO). Efficient *Lsd1* deletion in FACS isolated CKO splenic nB and $CD138^+$ PB was observed (Supplemental Fig. 1A), and *Lsd1* mRNA levels were decreased significantly in CKO nB and PB populations (Supplemental Fig. 1B).

Splenic B cells from naive CKO mice and $Cd19^{Cre/+}$ control mice (CreWT) were purified and cultured *ex vivo* in the presence of LPS, IL-2, and IL-5 (24) to induce differentiation. Flow cytometry performed at day three showed that CKO B cell cultures exhibited a significant reduction in the frequency and total number of $CD138^+$ PB (Fig. 2A). Secreted antibody measured by ELISA from the same cultures showed a significant reduction in secreted IgM in CKO as compared to CreWT (Fig. 2B). The reduced number of PB was not due to cell death as CKO and CreWT B cell cultures showed no difference in the frequency of apoptotic or necrotic cells (Supplemental Fig. 2A). The consequence of *in vivo Lsd1* deletion on B cell differentiation was assessed by inoculating CKO and CreWT mice with LPS and analyzing spleens at the peak B cell response time point of three days (41).

Compared to CreWT mice, CKO mice exhibited a significant reduction in the frequency and total number of $CD138^+$ PB, as well as a significant reduction in serum IgM titres (Fig. 2C, D). Consistent with the *ex vivo* data, this defect was not due to an increase in cell death as CKO and CreWT spleens showed no difference in apoptotic or necrotic nB and PB (Supplemental Fig. 2B). The defect was not due to a decrease in B cell activation as there was no difference in splenic $GL7^+$ activated B cells (Supplemental Fig. 2C). To assess whether LSD1 only functions in LPS-stimulated B cell differentiation, CKO and CreWT mice were inoculated with the A/PR8/34 (PR8) strain of influenza. At seven days post infection, mice were sacrificed and the mediastinal lymph nodes were harvested and analyzed. Flow cytometry showed a significant reduction in PB formed by both frequency and total number in CKO mice (Supplemental Fig. 2D). ELISA showed a significant reduction in IgM titers in the serum (Supplemental Fig. 2E). These data indicate that LSD1 is required for normal B cell differentiation.

The intrinsic nature of the defect was examined by purifying and adoptively transferring congenically marked CKO (CD45.1) and CreWT (CD45.1/2) splenic B cells in a 1:1 ratio into μMT (CD45.2) host mice, which lack B cells (42). Hosts were inoculated with LPS one day after transfer, and spleens were harvested and analyzed at day three. Compared to the CreWT B cell compartment, the CKO B cell compartment exhibited a significant reduction in the frequency and total number of $CD138^+$ PB, respectively (Fig. 2E). Together, these data show that the requirement of LSD1 for normal B cell differentiation is intrinsic to the adoptively transferred B cells.

The above results were further supported by breeding *Lsd1* floxed alleles to the tamoxifen-inducible *Rosa26*$^{CreERT2/+}$ allele (23) (IKO). Efficient *Lsd1* deletion in IKO splenic naïve B cells was achieved compared to WT cells after tamoxifen treatment (Supplemental Fig. 1C). Purified splenic B cells from naïve IKO mice and WT mice following tamoxifen treatment were cultured *ex vivo* as above. Similar to the CKO B cells, IKO B cells exhibited a significant reduction in PB formation and secreted IgM as compared to their respective controls (Fig. 2F, G). Because the IKO system deletes *Lsd1* from all cells within the mouse, the effect of *Lsd1* deletion on B cells was tested by purifying splenic B cells from tamoxifen-treated IKO and WT mice and transferring them separately into μMT host mice. Following LPS inoculation and analysis as above, host mice that received IKO B cells again exhibited a significant reduction in the frequency and total number of PB, respectively (Fig. 2H). ELISA was performed on host serum and revealed that IKO cell recipient hosts had a significant reduction in serum IgM titres (Fig. 2I). Thus, ablation of LSD1 using multiple mechanisms of genetic deletion demonstrated that B cell differentiation and humoral immune responses are impaired in the absence of LSD1 and this defect is cell-intrinsic.

LSD1 regulates the plasmablast transcriptional program

To elucidate the molecular program altered by LSD1 deficiency during PB formation, RNA-seq was performed on FACS isolated $B220^+GL7^-CD138^-$ nB and $CD138^+$ PB from both CKO and *Lsd1*$^{fl/fl}$ (WT) splenocytes three days after LPS inoculation. Hierarchical clustering and principal component analysis (PCA) of all expressed genes showed that samples stratified by both cell type and *Lsd1* deletion status, indicating an LSD1-dependent

effect in both nB and PB (Fig. 3A, B). Calculations of total mRNA per cell showed the expected increase in mRNA levels from nB to PB (9) but no difference between CKO and WT samples, indicating that *Lsd1* deletion did not affect global cellular mRNA levels (Fig. 3C). In the wild-type setting, 1,428 genes were downregulated and 6,050 genes were upregulated in PB as compared to nB (Fig. 3D, referred to hereafter as DEG groups 1R and 2R, respectively). Comparison between WT and CKO nB found 38 downregulated and 382 upregulated genes in CKO nB (DEG groups 3R and 4R, respectively). Likewise, comparison between CKO and WT PB identified 41 downregulated and 471 upregulated genes in CKO PB (DEG groups 5R and 6R, respectively). These data show that LSD1 predominantly functions as a transcriptional repressor in this system and identify genes that are dysregulated in its absence.

The global functions of LSD1-dysregulated genes were investigated by performing Gene Ontology (GO) analysis on DEG groups (Supplemental Fig. 3A). The top enriched GO term for 6R DEG was immune system process. This was further supported by gene set enrichment analysis (GSEA) of the WT and CKO PB RNA-seq data comparisons to all HALLMARK and KEGG gene sets (Supplemental Fig. 3B), which revealed that genes involved in processes such as the inflammatory response, cell signaling, complement cascade, coagulation, cellular adhesion, and cytokine-cytokine receptor interactions were upregulated in the absence of LSD1. For example, LSD1-deficient PB upregulated the pro-inflammatory genes *C1qa*, *C1qb*, *C1qc*, *C3*, *C4bp*, *Cd14*, and *Tlr7*, as well as the IFN-γ response genes *Ifit2*, *Ifitm3*, *Il10ra*, *Usp18*, *Vamp5*, and *Vcam1*. These data therefore show that LSD1 normally represses pro-inflammatory signals during B cell differentiation.

Interestingly, the top enriched GO term (immune system process) for genes upregulated in CKO PB compared to WT controls (1R) matched the top GO term for genes downregulated in WT PB compared to WT nB (6R). This implies that genes downregulated when cells normally differentiate from nB to PB were derepressed in the absence of LSD1. This was also supported by the finding that between DEG groups 1R (normally repressed in PB) and 6R (upregulated in CKO PB) there were 143 genes that overlapped, which was 2.5-fold more than expected by chance (Supplemental Fig. 3C). No significant overlap was observed between 1R and 5R (Supplemental Fig. 3C). To further examine the derepressed genes, genes were ranked by expression differences between WT and CKO PB and compared to the 200 most significant DEG from 1R (genes repressed in PB) using GSEA (Fig. 3E). This analysis showed that genes aberrantly upregulated in CKO PB were significantly enriched for genes normally repressed in WT PB, further underscoring the importance of LSD1 in gene repression during PB formation. Additional analyses using gene sets defining follicular splenic B cells and plasma cells (7) corroborated the above GSEA results (Supplemental Fig. 3D). Example genes that exhibited this expression pattern included those that function in complement activation (*Cfp* (43)), homing (*Itgb7* (44), *Sell* (45)), response to bacteria (*Mpeg1* (46)), signaling (*Lsp1* (47), *Plaur* (48), *Siglecg* (49)), and survival (*Gimap4* (50); Fig. 3F). These results were validated by qRT-PCR with CreWT control cells, confirming a significant derepression in CKO PB (Supplemental Fig. 3E).

GSEA performed with the top 200 up DEG from group 2R (normally upregulated in PB) revealed that some genes in WT PB were superinduced in the absence of LSD1 (Fig. 3G),

which was validated as above (Supplemental Fig. 3D). Example genes that exhibited this expression pattern included *Ly6c*, which encodes a plasma cell surface marker (51), and those that function in adhesion (*Amigo2* (52)), homing (*Cd68* (53)), proliferation (*Cd300a* (54), *Uchl1* (55)), response to virus (*Ifitm3* (56)), and signaling (*Cd28* (57), *Dusp14* (58); Fig. 3H). These results were validated with qRT-PCR as above, confirming significant superinduction (Supplemental Fig. 3F), and highlight LSD1 as a transcriptional rheostat throughout B cell differentiation.

Blimp-1 target repressed genes are regulated by LSD1

One possible explanation for the transcriptional dysregulation observed in CKO PB is LSD1-dependent dysregulation of essential transcription factors. However, this did not appear to be the case as genes encoding nB transcription factors (BACH2, BCL6, ETS1, IRF8, PAX5, SPIB) and PB transcription factors (Blimp-1, IRF4, XBP-1) were appropriately expressed and regulated (Supplemental Fig. 3G). However, Blimp-1 has been shown to recruit histone modifying complexes to facilitate gene repression (10) and can physically interact with LSD1 (20). To determine if direct Blimp-1 target genes were dysregulated when LSD1 was deleted, Blimp-1 activated and repressed gene sets (10) were tested for enrichment in ranked gene lists derived from the comparisons nB WT vs. PC WT; nB WT vs. nB CKO; and PB WT vs. PB CKO (Fig. 4A). As expected in the wild-type setting, the GSEA of WT nB and PB identified genes up and down regulated by Blimp-1 (Fig. 4A, top). No enrichment involving Blimp-1 target genes was observed when comparing WT and CKO nB (Fig. 4A, middle). In contrast, when comparing WT and CKO PB, Blimp-1 repressed target genes failed to be fully downregulated (Fig. 4A, bottom), suggesting that LSD1 deficiency leads to derepression of Blimp-1 target genes. Examples included the genes *Mpeg1* and *Sell* as described above (Fig. 3F), a gene encoding a glycoprotein found in neutrophil azurophilic granules with putative amidase activity (*Plbd1* (59)), and those involved in response to bacteria (*Tlr1* (60)) and signaling (*Evl* (61), *Hck* (62), *Hvcn1* (63), *Il10ra* (64); Fig. 4B). Gene expression levels were validated with qRT-PCR as above and confirmed significant derepression in CKO PB (Supplemental Fig. 3H). These data indicate that LSD1 is, in part, responsible for repressing genes inhibited by Blimp-1.

LSD1 promotes B cell proliferation

Annotation of differentially expressed genes to HALLMARK and KEGG gene sets by GSEA identified proliferation and cell cycle genes downregulated in CKO PB as compared to WT (Supplemental Fig. 4A). This is consistent with fewer PB observed following LPS-mediated *in vivo* B cell differentiation, suggesting that LSD1 may regulate B cell proliferation. To test if there was a proliferation defect, the proliferative capacity of CreWT and CKO B cells in response to LPS was quantified by CTV staining of purified splenic B cells that were cultured *ex vivo* as above. Cultures were analyzed at 24, 36, 48, 60, and 72 hours (Fig. 5A **and** Supplemental Fig. 4B). CKO B cell cultures accumulated significantly fewer cells at 60 and 72 hours compared to CreWT B cell cultures. Moreover, when assessed by division, CKO cultures produced fewer total cells after 36 hours and fewer $CD138^{+}$ PB at all time points after 24 hours of culture.

The *in vivo* proliferation defect was characterized by purifying CKO and CreWT B cells, staining them with CTV, and adoptively transferring them into a μMT host and inoculating them with LPS as above. CKO cells had significantly reduced cells in divisions two through nine, and the total number of $CD138^+$ PB in later divisions was decreased substantially (Fig 5B.). Together, these data indicate that LSD1 is critical for normal B cell proliferation in response to LPS.

LSD1 regulates chromatin accessibility at ETS and IRF transcription factor motifs

ATAC-seq was performed on the same samples as RNA-seq to assess the global effects of LSD1 deficiency on active regulatory elements during B cell differentiation. PCA of ATAC-seq data showed that samples stratified by both cell type and *Lsd1* deletion status (Fig. 6A), supporting a chromatin regulatory role for LSD1 in nB and PB. Differential accessibility analysis indicated that in the wild-type setting, PB lost 19,461 and gained 12,646 accessibility regions compared to nB (Fig. 6B, referred to hereafter to as differentially accessible region (DAR) groups 1A and 2A, respectively). Examining WT and CKO sample comparisons of the same cell type found that both CKO nB and CKO PB underwent mostly targeted increases in chromatin accessibility (groups 4A and 6A, respectively).

To gain insight into the transcription factors associated with LSD1-regulated chromatin in PB, motif analysis (35) was performed on DAR groups 1A, 2A, and 6A (Fig. 6C). Group 1A DAR, which contained nB-accessible regions that normally would be inaccessible in PB, were enriched for motifs of transcription factors known to be important in nB development and maturation, including ETS1 (65), RUNX1 (66), and PAX5 (67). Group 2A DAR, which contained newly accessible regions in PB, were enriched for motifs of transcription factors known to be important for plasma cell formation and function, including E2A (68), OCT2 (69), and IRF4 (70). Group 6A DAR, which were more accessible due to loss of LSD1, were primarily enriched for motifs of the transcription factor families ETS and IRF and were modestly enriched for motifs of the transcription factor families MADS and POU, suggesting that LSD1 functions to restrict chromatin accessibility at the binding sites of these factors. The occurrence of several motifs, including E2F1, Sox2, and Sox3 do not occur in any of the DAR groups (Fig. 6C), suggesting specificity for the identified motifs. Example 6A DAR that contained motifs of transcription factors belonging to these families and that also mapped to a 6R DEG are displayed (Fig. 6D; *Arpp21*, *Atp10a*, *Med12l*, *Per3*, *Serpina3g, Slc16a7*). Overall, these data link PB-based chromatin closure with LSD1 at sites enriched with ETS, IRF, MADS, and POU family motifs and suggests a functional relationship between LSD1 and transcription factors of these families.

LSD1 restricts chromatin accessibility at naïve B cell enhancers in plasmablasts

Analysis of DAR revealed a 2.05-fold more than expected overlap between DAR groups 6A and 1A compared to no significant overlap between groups 5A and 1A, indicating that LSD1 restricts chromatin accessibility at regions normally accessible in nB (Fig 7A). To determine if LSD1-specific DAR occurred at nB regulatory regions, 1A, 2A, and 6A DAR were analyzed for enrichment of the active chromatin histone modifications H3K4me1 and H3K27ac from published nB datasets (71) (Fig 7B). Compared to 2A, both 1A and 6A DAR were significantly enriched for both marks, suggesting that in nB, 1A and 6A DAR were

located at cis-regulatory elements. The overlap of DAR and active enhancers (containing H3K4me1 and H3K27ac, but not H3K4me3 (72)) in several cell types was assessed by an odds ratio (Fig. 7C). The analysis indicated that 1A, 2A, and 6A DAR significantly overlapped active enhancers from various cell types, which is expected given that enhancers can be shared between cell types (73), but the highest degree of overlap for 1A and 6A DAR was observed with nB active enhancers. Conversely, DAR rarely occurred at active promoters (containing H3K27ac and H3K4me3, but not H3K4me1). nB active enhancers overlapping with 1A, 2A, and 6A DAR were tested for enrichment of H3K4me2 in wild-type nB and PB cells (Fig. 7D). Both 1A and 6A nB enhancers exhibited a significant decrease in H3K4me2 whereas 2A nB enhancers exhibited a significant increase, demonstrating that 1A and 6A nB enhancer regions normally lose LSD1-target H3K4 methylation in PB. Overall, these data imply that LSD1 functions to decommission nB active enhancers.

Motif analysis was performed on 1A and 6A nB enhancers to gain insight into the transcription factors possibly bound at LSD1-regulated nB enhancers (Fig. 7E). In both enhancer sets, the most significantly enriched motifs included ETS and IRF family factors. These data suggest that LSD1 restricts chromatin accessibility at enhancers containing ETS and IRF motifs during PB differentiation.

The relationship between LSD1 and transcription factors was explored by analyzing published ChIP-seq data for the factors PU.1, IRF4, and Blimp-1 from *ex vivo* LPS-induced PB (10). PU.1 was chosen because it is an ETS family transcription factor known to regulate the development and differentiation of B cells and also interact with IRF factors (5, 74). IRF4 was chosen because of its clear and critical role during B cell differentiation (70). All binding sites per transcription factor were analyzed for H3K4me2 enrichment in wild-type nB and PB (Supplemental Fig. 5A). All three sets of binding sites exhibited a significant decrease in H3K4me2, suggesting a role for LSD1 at these sites. Binding of the each of the above factors was found to occur within the 594 group 6A DAR (170, 17, 34, respectively), suggesting that these transcription factors bind at LSD1-regulated chromatin and potentially contribute to the recruitment of LSD1 (Supplemental Fig. 5B). These results do not preclude the action of additional factors from influencing LSD1-regulated chromatin.

The role of LSD1 at PU.1, IRF4, and Blimp-1 binding sites that map to LSD1-regulated genes were examined. To start, transcription factor binding sites were mapped to within 100 kb of genes upregulated in LSD1-deficient PB (6R DEG), resulting in three distinct groups of transcription factor binding sites (6R PU.1, 512 binding sites; 6R IRF4, 290 binding sites; 6R Blimp-1, 144 binding sites). Each group was assessed for enrichment of the LSD1-target histone modification H3K4me2 in wild-type nB and PB (10, 40) (Fig. 7F). The analysis found that H3K4me2 levels decreased in PB compared to nB for all three groups, suggesting a role for LSD1 at these sites. To explore this further, chromatin accessibility data from this study were examined similarly (Fig. 7G). Each of the three transcription factor binding site groups exhibited a significant increase in chromatin accessibility in LSD1-deficient PB. For a negative control, regions that were bound by SOX2, a transcription factor not involved in regulating B cell differentiation (75), were analyzed as above (6R SOX2, 294 binding sites; Supplemental Fig. 5C, 5D). No significant differences were found. Example PU.1, IRF4,

and Blimp-1 transcription factor binding sites identified in the above analyses are displayed (Fig. 7H; *Hmgcll1*, *L3mbtl3*, *Timd2*). These data support a chromatin remodeling role for LSD1 at PU.1, IRF4, and Blimp-1 target binding sites that map to LSD1-regulated genes.

Aberrant accumulation of H3K4me1 at LSD1-regulated loci

The effect that LSD1 had on chromatin accessibility during B cell differentiation was mainly restrictive and occurred at enhancer regions, implying that LSD1 demethylates the active enhancer histone modification H3K4me1 in this system. To determine if this was the case, H3K4me1 levels at LSD1-regulated DAR (Fig. 6, **group 6A**) were assayed by ChIP. Chromatin was prepared from CreWT nB, CKO nB, CreWT PB, and CKO PB and H3K4me1 ChIP-qPCR was performed on a set of nine regions previously defined (Fig. 6D, 7H). Regions mapping to the derepressed genes *Med12l*, *Slc16a7*, and *L3mbtl3* and the superinduced genes *Arpp21*, *Atp10a*, *Per3*, and *Hmgcll1* exhibited significant increases in H3K4me1 in CKO PB compared to CreWT PB (Fig. 8A, Supplemental Fig. 6A, 6B). Of these DAR, those that mapped to the genes *Arpp21*, *Atp10a*, *Hmgcll1*, and *L3mbtl3* mapped to a nB active enhancer (Fig. 7C).

To further explore the role of LSD1 in regulating H3K4me1, twelve additional potential enhancer regions mapping to LSD1-regulated genes (Fig. 3F, 3H, 4B) were chosen based on 1) transcription factor binding of PU.1, Blimp-1, or IRF4; and 2) presence of H3K4me1 in nB reported previously (10, 71). Regions mapping to the derepressed genes *Hck*, *Sell*, and *Siglecg*, and the superinduced genes *Amigo2*, *Cd28*, and *Ifitm3* exhibited significant increases in H3K4me1 in PB in the absence of LSD1 (Fig. 8B, Supplemental Fig. 6C). Five out of six regions, including all three derepressed gene genes, mapped to a nB active enhancer (Supplemental Fig. 6D). Other regions did not reach statistical significance for increases in H3K4me1 in the absence of LSD1, suggesting that the role of LSD1 is specific to certain regions.

Some of the regions significant for H3K4me1 increases were further examined in the context of other model systems. Using *in vitro*-derived effector $CD8^+$ T cell ChIP-seq data of the enhancer modifications H3K4me1 and H3K27ac, as well as IRF4 binding (76), four regions were identified as IRF4-bound enhancers (Supplemental Fig. 7A). *Ifitm3* and *L3mbtl3* were identified as responsive to changes in IRF4 expression in $IRF4^{-/+}$ exhausted $CD8^+$ T cells (77). *Atp10a* and *Siglecg* were identified as being bound by BATF and NFAT in addition to IRF4 and represent chronic infection signature genes (77). Using ATAC-seq data and PU.1 and LSD1 ChIP-seq data from mouse-engrafted MLL-AF9 primary acute myeloid leukemia cells either treated or not treated with an LSD1 inhibitor (78), regions mapping to *Serpina3g*, *Ifitm3*, *L3mbtl3*, and *Siglecg* were identified as being bound by LSD1, PU.1, and exhibiting increased accessibility upon pharmacological inhibition of LSD1 (Supplemental Fig. 7B). These analyses support our conclusions that the regions examined represent regulatory regions that LSD1 decommissions.

Discussion

This study demonstrates a critical *in vivo* role for LSD1 during B cell differentiation in response to the T cell-independent antigen LPS. In LSD1-deficient PB, derepression and

superinduction of immune system process genes was observed with some derepressed genes being targets of Blimp-1 repression. LSD1 also positively regulated the expression of cell cycle genes, which was concordant with a decrease in proliferation upon LSD1 deletion. Mechanistically, LSD1-regulated chromatin accessibility and H3K4me1 levels at many but not all nB active enhancers and PU.1, IRF4, and Blimp-1 binding sites mapping to LSD1-repressed genes as the cells differentiated to PB. Together, these data show that LSD1 modulates PB transcriptional networks through epigenetic reprogramming.

LSD1 deletion resulted in the derepression and superinduction of hundreds of genes in PB. Previous studies have shown that LSD1 deletion results in gene derepression through failure to remove H3K4 methylation (15, 17). This same observation was noted for just more than half of the genes/regions assessed here. Some of the regions that showed increased H3K4me1 in the absence of LSD1 mapped to DAR. Together, these observations suggest that there may be multiple mechanisms that allow the decommissioning of active enhancer regions with the first mechanism relying on LSD1 to demethylate active histone H3K4me1/2 modification and functioning as a regulator of chromatin accessibility. Additional mechanisms may rely on other demethylases that belong to the JARID/Jumanji family of proteins (79).

LSD1 deletion in B cells caused a compound effect of decreased proliferation and differentiation. This was not due to increased cell death or a defect in B cell activation. Decreased proliferation and differentiation were also observed in an *ex vivo* B cell differentiation culture system, arguing against defective *in vivo* homing. The data cannot rule out that reduced proliferation contributed to reduced differentiation but given that LSD1 modulates the expression of hundreds of non-cell cycle genes, it is likely that other factors are contributing to the phenotype. For example, CD28-deficient B cells produce more short- and long-lived plasma cells (80); thus CD28 overexpression observed in this system may result in fewer PB. Also, it may be possible that certain gene regulatory effects of LSD1 that contributed to the phenotype were undetected since the RNA-seq experiment was performed only on the nB and PB stages and not any activated B cells from the divisions in between. Future comparisons between nB and activated B cells, as well as activated B cells to PB may shed additional light on the specific role of LSD1 during key stages of B cell differentiation.

The data display a proliferation defect, but both WT and CKO PB underwent a sufficient number of divisions within the same time period to differentiate. This indicates that the WT and LSD1-deficient cells proliferate to the same extent and argues that the gene expression and chromatin dysregulation observed is due to LSD1 deletion and not a reduced capacity to proliferate. The decreased expression of cell cycle genes corresponds with the phenotype, but the most substantial changes in gene expression were increases. Also, ATAC-seq and ChIP-qPCR data indicate that LSD1 primarily represses active chromatin. Together, these data argue against a role for LSD1 directly activating gene expression and indicate that the effect on cell cycle gene expression may be indirect. Cell cycle regulator genes such as *Rb1*, E2F family genes, or *Myc,* which have been observed in other systems to affect B cell differentiation (81, 82), were not aberrantly expressed, implying an alternative mechanism for cell cycle gene downregulation and reduced proliferation. A number of genes aberrantly upregulated in the absence of LSD1 may be contributing. For example, CD300a was

superinduced in LSD1-deficient PB. It has been shown CD300a negatively regulates BCR-stimulus-induced B cell proliferation (54), suggesting that overexpression in the LPS-stimulation model may dampen B cell proliferation.

Histone modifying enzymes are recruited to target sites through interaction with transcription factors (79). LSD1 interacts with numerous transcription factors (12, 18, 19), including Blimp-1 (20). Here, LSD1 deficiency resulted in the derepression of Blimp-1 target genes and an increase in chromatin accessibility at Blimp-1 target binding sites mapping to genes upregulated in LSD1-deficient PB, supporting a functional role for a Blimp-1-LSD1 interaction. The enrichment of LSD1-regulated nB active enhancers with ETS and IRF family motifs, as well as analyses with PU.1 and IRF4 binding sites mapping to LSD1-regulated genes suggests a functional relationship between LSD1 and these factors. This is also supported by LSD1-dependent modulation of H3K4me1 levels in CKO PB at certain target regions bound by these factors. Additional evidence that LSD1 regulates PU.1-target sites in B cells was presented in a study in which treatment of a mouse-engrafted acute myeloid leukemia cell line with an LSD1 inhibitor increased chromatin accessibility at PU.1-target enhancers (78). Both PU.1-IRF4 complexes and Blimp-1 can bind to ETS-IRF composite elements (EICEs) (10), highlighting the dynamic regulatory network between PU.1, IRF4, and Blimp-1 in PB; and given the evidence stated above, supports a role for LSD1 in regulating this network.

It is becoming increasingly clear that epigenetic remodeling is necessary for sufficient humoral responses. Epigenetic modifying proteins such EZH2 (11) and the de novo DNA methyltransferases DNMT3A and DNMT3B (83, 84) have been shown to play important roles in B cell proliferation and differentiation. Similar to LSD1 deficiency, B cell conditional deletion of EZH2 resulted in fewer LPS-derived PB and the aberrant overexpression of hundreds of genes (11). The EZH2-based reduction in PB was likely due to derepression of the cell cycle checkpoint inhibitor p21 (*Cdkn1a*), a gene that must also be repressed in order for germinal center B cells to form (85). p21 was not dysregulated in LSD1-deficient PB, indicating that the mechanisms by which LSD1 and EZH2 regulate proliferation and PB formation are likely different, yet equally important. In contrast, mice with B cell conditional deletion of DNMT3A and 3B that were inoculated with a protein antigen displayed an increase in germinal center B cells and PC, suggesting that in a T cell dependent response, DNA methylation is required to restrict the B cell program and control plasma cell differentiation. Intriguingly, demethylated H3K4 can be bound by DNMT3L, which in turn recruits DNMT3A and 3B to methylate the target loci and facilitate gene repression (86). Although the antigen systems in which LSD1 and DNMT3A/B were studied were different, these data suggest that the acquisition of DNA methylation may require LSD1 to demethylate H3K4me1 at enhancers first. Irrespective of the system, the action of multiple and distinct epigenetic pathways must act in harmony for B cells to differentiate to plasma cells. It is now evident that LSD1 serves as an epigenetic rheostat, controlling both the repression of the naïve B cell transcriptional program and maintaining the appropriate expression of plasma cell genes.

Supplementary Material

Refer to Web version on PubMed Central for supplementary material.

Acknowledgements

We acknowledge members of the Boss lab for scientific contributions and editorial input. We thank the Emory Flow Cytometry Core for FACS, the Emory Integrated Genomics Core for sequencing library QC, and the NYU Genome Technology center for Illumina sequencing.

This work was supported by the following NIH grants: R01 AI123733 and P01 AI125180 to J.M.B., T32 GM0008490 to R.R.H. and B.G.B., F31 AI131532 to R.R.H., and F31 AI112261 to B.G.B.

Abbreviations

ASC	antibody-secreting cells
ATAC-seq	assay for transposase-accessible chromatin sequencing
ChIP	chromatin immunoprecipitation
ChIP-qPCR	chromatin immunoprecipitation quantitative PCR
ChIP-seq	ChIP sequencing
CKO	*Lsd1*$^{fl/fl}$ *Cd19*$^{Cre/+}$ conditional knockout
CreWT	*Lsd1*$^{+/+}$ *Cd19*$^{Cre/+}$ wild-type
CTV	CellTrace Violet
DAR	differentially accessible region
DEG	differentially expressed gene
ELISA	enzyme-linked immunosorbent assay
enh	enhancer
ERCC	external RNA controls consortium
FACS	fluorescence-activated cell sorting
FC	fold change
FDR	false discovery rate
FSC	forward scatter
GO	gene ontology
GSEA	gene set enrichment analysis
H3K4me1	histone 3 lysine 4 monomethylation
H3K4me2	histone 3 lysine 4 dimethylation

H3K4me3	histone 3 lysine 4 trimethylation
H3K27ac	histone 3 lysine 27 acetylation
H3K27me3	histone 3 lysine 27 trimethylation
H3K9me1	histone 3 lysine 9 monomethylation
H3K9me2	histone 3 lysine 9 dimethylation
IKO	*Lsd1*$^{fl/fl}$ *Rosa26*$^{CreERT2/+}$ inducible knockout
LPS	lipopolysaccharide
LSD1	lysine-specific demethylase 1
nB	naïve B cells
PB	plasmablasts
PC	plasma cells
PCA	principal component analysis
qPCR	quantitative polymerase chain reaction
qRT-PCR	quantitative reverse transcription PCR
rpm	reads per million
rppm	reads per peak per million
SD	standard deviation
SSC	side scatter
TD	T cell-dependent
TI	T cell-independent
WT	*Lsd1*$^{fl/fl}$ wild-type

References

1. Nutt SL, Hodgkin PD, Tarlinton DM, and Corcoran LM. 2015 The generation of antibody-secreting plasma cells. Nat Rev Immunol 15: 160–171. [PubMed: 25698678]
2. Oracki SA, Walker JA, Hibbs ML, Corcoran LM, and Tarlinton DM. 2010 Plasma cell development and survival. Immunol Rev 237: 140–159. [PubMed: 20727034]
3. MacLennan IC, Toellner KM, Cunningham AF, Serre K, Sze DM, Zuniga E, Cook MC, and Vinuesa CG. 2003 Extrafollicular antibody responses. Immunol Rev 194: 8–18. [PubMed: 12846803]
4. Cerutti A, Cols M, and Puga I. 2013 Marginal zone B cells: virtues of innate-like antibody-producing lymphocytes. Nat Rev Immunol 13: 118–132. [PubMed: 23348416]
5. Carotta S, Willis SN, Hasbold J, Inouye M, Pang SH, Emslie D, Light A, Chopin M, Shi W, Wang H, Morse HC, 3rd, Tarlinton DM, Corcoran LM, Hodgkin PD, and Nutt SL. 2014 The transcription factors IRF8 and PU.1 negatively regulate plasma cell differentiation. J Exp Med 211: 2169–2181. [PubMed: 25288399]

6. Price MJ, Patterson DG, Scharer CD, and Boss JM. 2018 Progressive Upregulation of Oxidative Metabolism Facilitates Plasmablast Differentiation to a T-Independent Antigen. Cell Rep 23: 3152–3159. [PubMed: 29898388]
7. Shi W, Liao Y, Willis SN, Taubenheim N, Inouye M, Tarlinton DM, Smyth GK, Hodgkin PD, Nutt SL, and Corcoran LM. 2015 Transcriptional profiling of mouse B cell terminal differentiation defines a signature for antibody-secreting plasma cells. Nat Immunol 16: 663–673. [PubMed: 25894659]
8. Scharer CD, Barwick BG, Guo M, Bally APR, and Boss JM. 2018 Plasma cell differentiation is controlled by multiple cell division-coupled epigenetic programs. Nat Commun 9: 1698. [PubMed: 29703886]
9. Barwick BG, Scharer CD, Bally AP, and Boss JM. 2016 Plasma cell differentiation is coupled to division-dependent DNA hypomethylation and gene regulation. Nat Immunol 17: 1216–1225. [PubMed: 27500631]
10. Minnich M, Tagoh H, Bonelt P, Axelsson E, Fischer M, Cebolla B, Tarakhovsky A, Nutt SL, Jaritz M, and Busslinger M. 2016 Multifunctional role of the transcription factor Blimp-1 in coordinating plasma cell differentiation. Nat Immunol 17: 331–343. [PubMed: 26779602]
11. Guo M, Price MJ, Patterson DG, Barwick BG, Haines RR, Kania AK, Bradley JE, Randall TD, Boss JM, and Scharer CD. 2018 EZH2 Represses the B Cell Transcriptional Program and Regulates Antibody-Secreting Cell Metabolism and Antibody Production. J Immunol 200: 1039–1052. [PubMed: 29288200]
12. Metzger E, Wissmann M, Yin N, Muller JM, Schneider R, Peters AH, Gunther T, Buettner R, and Schule R. 2005 LSD1 demethylates repressive histone marks to promote androgen-receptor-dependent transcription. Nature 437: 436–439. [PubMed: 16079795]
13. Shi Y, Lan F, Matson C, Mulligan P, Whetstine JR, Cole PA, Casero RA, and Shi Y. 2004 Histone demethylation mediated by the nuclear amine oxidase homolog LSD1. Cell 119: 941–953. [PubMed: 15620353]
14. Maiques-Diaz A, and Somervaille TC. 2016 LSD1: biologic roles and therapeutic targeting. Epigenomics 8: 1103–1116. [PubMed: 27479862]
15. Whyte WA, Bilodeau S, Orlando DA, Hoke HA, Frampton GM, Foster CT, Cowley SM, and Young RA. 2012 Enhancer decommissioning by LSD1 during embryonic stem cell differentiation. Nature 482: 221–225. [PubMed: 22297846]
16. Sun G, Alzayady K, Stewart R, Ye P, Yang S, Li W, and Shi Y. 2010 Histone demethylase LSD1 regulates neural stem cell proliferation. Mol Cell Biol 30: 1997–2005. [PubMed: 20123967]
17. Kerenyi MA, Shao Z, Hsu YJ, Guo G, Luc S, O'Brien K, Fujiwara Y, Peng C, Nguyen M, and Orkin SH. 2013 Histone demethylase Lsd1 represses hematopoietic stem and progenitor cell signatures during blood cell maturation. Elife 2: e00633. [PubMed: 23795291]
18. Shi YJ, Matson C, Lan F, Iwase S, Baba T, and Shi Y. 2005 Regulation of LSD1 histone demethylase activity by its associated factors. Mol Cell 19: 857–864. [PubMed: 16140033]
19. Bennesch MA, Segala G, Wider D, and Picard D. 2016 LSD1 engages a corepressor complex for the activation of the estrogen receptor alpha by estrogen and cAMP. Nucleic Acids Res 44: 8655–8670. [PubMed: 27325688]
20. Su ST, Ying HY, Chiu YK, Lin FR, Chen MY, and Lin KI. 2009 Involvement of histone demethylase LSD1 in Blimp-1-mediated gene repression during plasma cell differentiation. Mol Cell Biol 29: 1421–1431. [PubMed: 19124609]
21. Rickert RC, Roes J, and Rajewsky K. 1997 B lymphocyte-specific, Cre-mediated mutagenesis in mice. Nucleic Acids Res 25: 1317–1318. [PubMed: 9092650]
22. Wang J, Scully K, Zhu X, Cai L, Zhang J, Prefontaine GG, Krones A, Ohgi KA, Zhu P, Garcia-Bassets I, Liu F, Taylor H, Lozach J, Jayes FL, Korach KS, Glass CK, Fu XD, and Rosenfeld MG. 2007 Opposing LSD1 complexes function in developmental gene activation and repression programmes. Nature 446: 882–887. [PubMed: 17392792]
23. Ventura A, Kirsch DG, McLaughlin ME, Tuveson DA, Grimm J, Lintault L, Newman J, Reczek EE, Weissleder R, and Jacks T. 2007 Restoration of p53 function leads to tumour regression in vivo. Nature 445: 661–665. [PubMed: 17251932]

24. Yoon HS, Scharer CD, Majumder P, Davis CW, Butler R, Zinzow-Kramer W, Skountzou I, Koutsonanos DG, Ahmed R, and Boss JM. 2012 ZBTB32 is an early repressor of the CIITA and MHC class II gene expression during B cell differentiation to plasma cells. J Immunol 189: 2393–2403. [PubMed: 22851713]
25. Ballesteros-Tato A, Leon B, Graf BA, Moquin A, Adams PS, Lund FE, and Randall TD. 2012 Interleukin-2 inhibits germinal center formation by limiting T follicular helper cell differentiation. Immunity 36: 847–856. [PubMed: 22464171]
26. Jiang L, Schlesinger F, Davis CA, Zhang Y, Li R, Salit M, Gingeras TR, and Oliver B. 2011 Synthetic spike-in standards for RNA-seq experiments. Genome Res 21: 1543–1551. [PubMed: 21816910]
27. Kim D, Pertea G, Trapnell C, Pimentel H, Kelley R, and Salzberg SL. 2013 TopHat2: accurate alignment of transcriptomes in the presence of insertions, deletions and gene fusions. Genome Biol 14: R36. [PubMed: 23618408]
28. Lawrence M, Huber W, Pages H, Aboyoun P, Carlson M, Gentleman R, Morgan MT, and Carey VJ. 2013 Software for computing and annotating genomic ranges. PLoS Comput Biol 9: e1003118. [PubMed: 23950696]
29. Robinson MD, McCarthy DJ, and Smyth GK. 2010 edgeR: a Bioconductor package for differential expression analysis of digital gene expression data. Bioinformatics 26: 139–140. [PubMed: 19910308]
30. Huang da W, Sherman BT, and Lempicki RA. 2009 Systematic and integrative analysis of large gene lists using DAVID bioinformatics resources. Nat Protoc 4: 44–57. [PubMed: 19131956]
31. Subramanian A, Tamayo P, Mootha VK, Mukherjee S, Ebert BL, Gillette MA, Paulovich A, Pomeroy SL, Golub TR, Lander ES, and Mesirov JP. 2005 Gene set enrichment analysis: a knowledge-based approach for interpreting genome-wide expression profiles. Proc Natl Acad Sci U S A 102: 15545–15550. [PubMed: 16199517]
32. Buenrostro JD, Giresi PG, Zaba LC, Chang HY, and Greenleaf WJ. 2013 Transposition of native chromatin for fast and sensitive epigenomic profiling of open chromatin, DNA-binding proteins and nucleosome position. Nat Methods 10: 1213–1218. [PubMed: 24097267]
33. Langmead B, Trapnell C, Pop M, and Salzberg SL. 2009 Ultrafast and memory-efficient alignment of short DNA sequences to the human genome. Genome Biol 10: R25. [PubMed: 19261174]
34. Zhang Y, Liu T, Meyer CA, Eeckhoute J, Johnson DS, Bernstein BE, Nusbaum C, Myers RM, Brown M, Li W, and Liu XS. 2008 Model-based analysis of ChIP-Seq (MACS). Genome Biol 9: R137. [PubMed: 18798982]
35. Heinz S, Benner C, Spann N, Bertolino E, Lin YC, Laslo P, Cheng JX, Murre C, Singh H, and Glass CK. 2010 Simple combinations of lineage-determining transcription factors prime cis-regulatory elements required for macrophage and B cell identities. Mol Cell 38: 576–589. [PubMed: 20513432]
36. Scharer CD, Blalock EL, Barwick BG, Haines RR, Wei C, Sanz I, and Boss JM. 2016 ATAC-seq on biobanked specimens defines a unique chromatin accessibility structure in naive SLE B cells. Sci Rep 6: 27030. [PubMed: 27249108]
37. Scharer CD, Choi NM, Barwick BG, Majumder P, Lohsen S, and Boss JM. 2015 Genome-wide CIITA-binding profile identifies sequence preferences that dictate function versus recruitment. Nucleic Acids Res 43: 3128–3142. [PubMed: 25753668]
38. Lohsen S, Majumder P, Scharer CD, Barwick BG, Austin JW, Zinzow-Kramer WM, and Boss JM. 2014 Common distal elements orchestrate CIITA isoform-specific expression in multiple cell types. Genes Immun 15: 543–555. [PubMed: 25101797]
39. Majumder P, Scharer CD, Choi NM, and Boss JM. 2014 B cell differentiation is associated with reprogramming the CCCTC binding factor-dependent chromatin architecture of the murine MHC class II locus. J Immunol 192: 3925–3935. [PubMed: 24634495]
40. Gyory I, Boller S, Nechanitzky R, Mandel E, Pott S, Liu E, and Grosschedl R. 2012 Transcription factor Ebf1 regulates differentiation stage-specific signaling, proliferation, and survival of B cells. Genes Dev 26: 668–682. [PubMed: 22431510]

41. North CM, Crawford RB, Lu H, and Kaminski NE. 2009 Simultaneous in vivo time course and dose response evaluation for TCDD-induced impairment of the LPS-stimulated primary IgM response. Toxicol Sci 112: 123–132. [PubMed: 19675145]

42. Kitamura D, Roes J, Kuhn R, and Rajewsky K. 1991 A B cell-deficient mouse by targeted disruption of the membrane exon of the immunoglobulin mu chain gene. Nature 350: 423–426. [PubMed: 1901381]

43. Hourcade DE 2006 The role of properdin in the assembly of the alternative pathway C3 convertases of complement. J Biol Chem 281: 2128–2132. [PubMed: 16301317]

44. Gorfu G, Rivera-Nieves J, Hoang S, Abbott DW, Arbenz-Smith K, Azar DW, Pizarro TT, Cominelli F, McDuffie M, and Ley K. 2010 Beta7 integrin deficiency suppresses B cell homing and attenuates chronic ileitis in SAMP1/YitFc mice. J Immunol 185: 5561–5568. [PubMed: 20926792]

45. Morrison VL, Barr TA, Brown S, and Gray D. 2010 TLR-mediated loss of CD62L focuses B cell traffic to the spleen during Salmonella typhimurium infection. J Immunol 185: 2737–2746. [PubMed: 20660707]

46. McCormack RM, de Armas LR, Shiratsuchi M, Fiorentino DG, Olsson ML, Lichtenheld MG, Morales A, Lyapichev K, Gonzalez LE, Strbo N, Sukumar N, Stojadinovic O, Plano GV, Munson GP, Tomic-Canic M, Kirsner RS, Russell DG, and Podack ER. 2015 Perforin-2 is essential for intracellular defense of parenchymal cells and phagocytes against pathogenic bacteria. Elife 4.

47. Jongstra-Bilen J, Wielowieyski A, Misener V, and Jongstra J. 1999 LSP1 regulates anti-IgM induced apoptosis in WEHI-231 cells and normal immature B-cells. Mol Immunol 36: 349–359. [PubMed: 10443999]

48. Vagnarelli P, Raimondi E, Mazzieri R, De Carli L, and Mignatti P. 1992 Assignment of the human urokinase receptor gene (PLAUR) to 19q13. Cytogenet Cell Genet 60: 197–199. [PubMed: 1324136]

49. Jellusova J, and Nitschke L. 2011 Regulation of B cell functions by the sialic acid-binding receptors siglec-G and CD22. Front Immunol 2: 96. [PubMed: 22566885]

50. Schnell S, Demolliere C, van den Berk P, and Jacobs H. 2006 Gimap4 accelerates T-cell death. Blood 108: 591–599. [PubMed: 16569770]

51. Wrammert J, Kallberg E, Agace WW, and Leanderson T. 2002 Ly6C expression differentiates plasma cells from other B cell subsets in mice. Eur J Immunol 32: 97–103. [PubMed: 11754008]

52. Li Z, Khan MM, Kuja-Panula J, Wang H, Chen Y, Guo D, Chen ZJ, Lahesmaa R, Rauvala H, and Tian L. 2017 AMIGO2 modulates T cell functions and its deficiency in mice ameliorates experimental autoimmune encephalomyelitis. Brain Behav Immun 62: 110–123. [PubMed: 28119027]

53. O'Reilly D, Quinn CM, El-Shanawany T, Gordon S, and Greaves DR. 2003 Multiple Ets factors and interferon regulatory factor-4 modulate CD68 expression in a cell type-specific manner. J Biol Chem 278: 21909–21919. [PubMed: 12676954]

54. Silva R, Moir S, Kardava L, Debell K, Simhadri VR, Ferrando-Martinez S, Leal M, Pena J, Coligan JE, and Borrego F. 2011 CD300a is expressed on human B cells, modulates BCR-mediated signaling, and its expression is down-regulated in HIV infection. Blood 117: 5870–5880. [PubMed: 21482706]

55. Rolen U, Freda E, Xie J, Pfirrmann T, Frisan T, and Masucci MG. 2009 The ubiquitin C-terminal hydrolase UCH-L1 regulates B-cell proliferation and integrin activation. J Cell Mol Med 13: 1666–1678. [PubMed: 20187292]

56. Desai TM, Marin M, Chin CR, Savidis G, Brass AL, and Melikyan GB. 2014 IFITM3 restricts influenza A virus entry by blocking the formation of fusion pores following virus-endosome hemifusion. PLoS Pathog 10: e1004048. [PubMed: 24699674]

57. Rozanski CH, Utley A, Carlson LM, Farren MR, Murray M, Russell LM, Nair JR, Yang Z, Brady W, Garrett-Sinha LA, Schoenberger SP, Green JM, Boise LH, and Lee KP. 2015 CD28 Promotes Plasma Cell Survival, Sustained Antibody Responses, and BLIMP-1 Upregulation through Its Distal PYAP Proline Motif. J Immunol 194: 4717–4728. [PubMed: 25833397]

58. Yang CY, Li JP, Chiu LL, Lan JL, Chen DY, Chuang HC, Huang CY, and Tan TH. 2014 Dual-specificity phosphatase 14 (DUSP14/MKP6) negatively regulates TCR signaling by inhibiting TAB1 activation. J Immunol 192: 1547–1557. [PubMed: 24403530]

59. Repo H, Kuokkanen E, Oksanen E, Goldman A, and Heikinheimo P. 2014 Is the bovine lysosomal phospholipase B-like protein an amidase? Proteins 82: 300–311. [PubMed: 23934913]

60. Takeuchi O, Sato S, Horiuchi T, Hoshino K, Takeda K, Dong Z, Modlin RL, and Akira S. 2002 Cutting edge: role of Toll-like receptor 1 in mediating immune response to microbial lipoproteins. J Immunol 169: 10–14. [PubMed: 12077222]

61. Krause M, Sechi AS, Konradt M, Monner D, Gertler FB, and Wehland J. 2000 Fyn-binding protein (Fyb)/SLP-76-associated protein (SLAP), Ena/vasodilator-stimulated phosphoprotein (VASP) proteins and the Arp2/3 complex link T cell receptor (TCR) signaling to the actin cytoskeleton. J Cell Biol 149: 181–194. [PubMed: 10747096]

62. Poh AR, O'Donoghue RJ, and Ernst M. 2015 Hematopoietic cell kinase (HCK) as a therapeutic target in immune and cancer cells. Oncotarget 6: 15752–15771. [PubMed: 26087188]

63. Capasso M, Bhamrah MK, Henley T, Boyd RS, Langlais C, Cain K, Dinsdale D, Pulford K, Khan M, Musset B, Cherny VV, Morgan D, Gascoyne RD, Vigorito E, DeCoursey TE, MacLennan IC, and Dyer MJ. 2010 HVCN1 modulates BCR signal strength via regulation of BCR-dependent generation of reactive oxygen species. Nat Immunol 11: 265–272. [PubMed: 20139987]

64. Walter MR 2014 The molecular basis of IL-10 function: from receptor structure to the onset of signaling. Curr Top Microbiol Immunol 380: 191–212. [PubMed: 25004819]

65. Saelee P, Kearly A, Nutt SL, and Garrett-Sinha LA. 2017 Genome-Wide Identification of Target Genes for the Key B Cell Transcription Factor Ets1. Front Immunol 8: 383. [PubMed: 28439269]

66. Niebuhr B, Kriebitzsch N, Fischer M, Behrens K, Gunther T, Alawi M, Bergholz U, Muller U, Roscher S, Ziegler M, Buchholz F, Grundhoff A, and Stocking C. 2013 Runx1 is essential at two stages of early murine B-cell development. Blood 122: 413–423. [PubMed: 23704093]

67. Horcher M, Souabni A, and Busslinger M. 2001 Pax5/BSAP maintains the identity of B cells in late B lymphopoiesis. Immunity 14: 779–790. [PubMed: 11420047]

68. Wohner M, Tagoh H, Bilic I, Jaritz M, Poliakova DK, Fischer M, and Busslinger M. 2016 Molecular functions of the transcription factors E2A and E2–2 in controlling germinal center B cell and plasma cell development. J Exp Med 213: 1201–1221. [PubMed: 27261530]

69. Hodson DJ, Shaffer AL, Xiao W, Wright GW, Schmitz R, Phelan JD, Yang Y, Webster DE, Rui L, Kohlhammer H, Nakagawa M, Waldmann TA, and Staudt LM. 2016 Regulation of normal B-cell differentiation and malignant B-cell survival by OCT2. Proc Natl Acad Sci U S A 113: E2039–2046. [PubMed: 26993806]

70. Klein U, Casola S, Cattoretti G, Shen Q, Lia M, Mo T, Ludwig T, Rajewsky K, and Dalla-Favera R. 2006 Transcription factor IRF4 controls plasma cell differentiation and class-switch recombination. Nat Immunol 7: 773–782. [PubMed: 16767092]

71. Sabo A, Kress TR, Pelizzola M, de Pretis S, Gorski MM, Tesi A, Morelli MJ, Bora P, Doni M, Verrecchia A, Tonelli C, Faga G, Bianchi V, Ronchi A, Low D, Muller H, Guccione E, Campaner S, and Amati B. 2014 Selective transcriptional regulation by Myc in cellular growth control and lymphomagenesis. Nature 511: 488–492. [PubMed: 25043028]

72. Creyghton MP, Cheng AW, Welstead GG, Kooistra T, Carey BW, Steine EJ, Hanna J, Lodato MA, Frampton GM, Sharp PA, Boyer LA, Young RA, and Jaenisch R. 2010 Histone H3K27ac separates active from poised enhancers and predicts developmental state. Proc Natl Acad Sci U S A 107: 21931–21936. [PubMed: 21106759]

73. Lara-Astiaso D, Weiner A, Lorenzo-Vivas E, Zaretsky I, Jaitin DA, David E, Keren-Shaul H, Mildner A, Winter D, Jung S, Friedman N, and Amit I. 2014 Immunogenetics. Chromatin state dynamics during blood formation. Science 345: 943–949. [PubMed: 25103404]

74. Torlakovic E, Tierens A, Dang HD, and Delabie J. 2001 The transcription factor PU.1, necessary for B-cell development is expressed in lymphocyte predominance, but not classical Hodgkin's disease. Am J Pathol 159: 1807–1814. [PubMed: 11696441]

75. Matsuda K, Mikami T, Oki S, Iida H, Andrabi M, Boss JM, Yamaguchi K, Shigenobu S, and Kondoh H. 2017 ChIP-seq analysis of genomic binding regions of five major transcription factors

highlights a central role for ZIC2 in the mouse epiblast stem cell gene regulatory network. Development 144: 1948–1958. [PubMed: 28455373]

76. Kurachi M, Barnitz RA, Yosef N, Odorizzi PM, DiIorio MA, Lemieux ME, Yates K, Godec J, Klatt MG, Regev A, Wherry EJ, and Haining WN. 2014 The transcription factor BATF operates as an essential differentiation checkpoint in early effector CD8+ T cells. Nat Immunol 15: 373–383. [PubMed: 24584090]
77. Man K, Gabriel SS, Liao Y, Gloury R, Preston S, Henstridge DC, Pellegrini M, Zehn D, Berberich-Siebelt F, Febbraio MA, Shi W, and Kallies A. 2017 Transcription Factor IRF4 Promotes CD8(+) T Cell Exhaustion and Limits the Development of Memory-like T Cells during Chronic Infection. Immunity 47: 1129–1141 e1125. [PubMed: 29246443]
78. Cusan M, Cai SF, Mohammad HP, Krivtsov A, Chramiec A, Loizou E, Witkin MD, Smitheman KN, Tenen DG, Ye M, Will B, Steidl U, Kruger RG, Levine RL, Rienhoff HY, Jr., Koche RP, and Armstrong SA. 2018 LSD1 inhibition exerts its anti-leukemic effect by recommissioning PU.1- and C/EBPalpha-dependent enhancers in AML. Blood.
79. Kooistra SM, and Helin K. 2012 Molecular mechanisms and potential functions of histone demethylases. Nat Rev Mol Cell Biol 13: 297–311. [PubMed: 22473470]
80. Njau MN, Kim JH, Chappell CP, Ravindran R, Thomas L, Pulendran B, and Jacob J. 2012 CD28-B7 interaction modulates short- and long-lived plasma cell function. J Immunol 189: 2758–2767. [PubMed: 22908331]
81. Shaffer AL, Lin KI, Kuo TC, Yu X, Hurt EM, Rosenwald A, Giltnane JM, Yang L, Zhao H, Calame K, and Staudt LM. 2002 Blimp-1 orchestrates plasma cell differentiation by extinguishing the mature B cell gene expression program. Immunity 17: 51–62. [PubMed: 12150891]
82. Lam EW, Glassford J, van der Sman J, Banerji L, Pizzey AR, Shaun N, Thomas B, and Klaus GG. 1999 Modulation of E2F activity in primary mouse B cells following stimulation via surface IgM and CD40 receptors. Eur J Immunol 29: 3380–3389. [PubMed: 10540350]
83. Barwick BG, Scharer CD, Martinez RJ, Price MJ, Wein AN, Haines RR, Bally APR, Kohlmeier JE, and Boss JM. 2018 B cell activation and plasma cell differentiation are inhibited by de novo DNA methylation. Nat Commun 9: 1900. [PubMed: 29765016]
84. Lai AY, Mav D, Shah R, Grimm SA, Phadke D, Hatzi K, Melnick A, Geigerman C, Sobol SE, Jaye DL, and Wade PA. 2013 DNA methylation profiling in human B cells reveals immune regulatory elements and epigenetic plasticity at Alu elements during B-cell activation. Genome Res 23: 2030–2041. [PubMed: 24013550]
85. Beguelin W, Rivas MA, Calvo Fernandez MT, Teater M, Purwada A, Redmond D, Shen H, Challman MF, Elemento O, Singh A, and Melnick AM. 2017 EZH2 enables germinal centre formation through epigenetic silencing of CDKN1A and an Rb-E2F1 feedback loop. Nat Commun 8: 877. [PubMed: 29026085]
86. Ooi SK, Qiu C, Bernstein E, Li K, Jia D, Yang Z, Erdjument-Bromage H, Tempst P, Lin SP, Allis CD, Cheng X, and Bestor TH. 2007 DNMT3L connects unmethylated lysine 4 of histone H3 to de novo methylation of DNA. Nature 448: 714–717. [PubMed: 17687327]

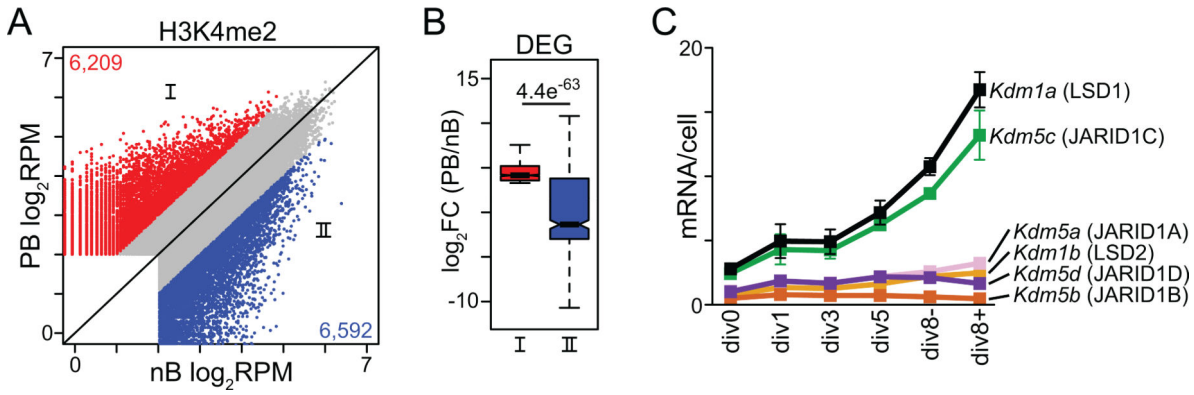

Figure 1 –. H3K4me2 is remodeled throughout B cell differentiation.

(A) Scatter plot of genomic regions significantly enriched for H3K4me2 in naïve B cells and LPS-induced plasmablasts (37,887 total peaks). Regions that gain or lose H3K4me2 in PB by a $\log_2$ fold change of at least one are red and blue, respectively. **(B)** Box plots of the $\log_2$ fold change of the expression of genes differentially expressed from naïve B cells vs. LPS-induced plasmablasts that map within 20 kB of at least one H3K4me2 peak within PB up regions (red box, I) and PB down regions (blue box, II). Significance determined by Wilcoxon rank sum test. **(C)** Expression in mRNA/cell per division of known H3K4me2 demethylases(9). Error bars represent mean ± SD.

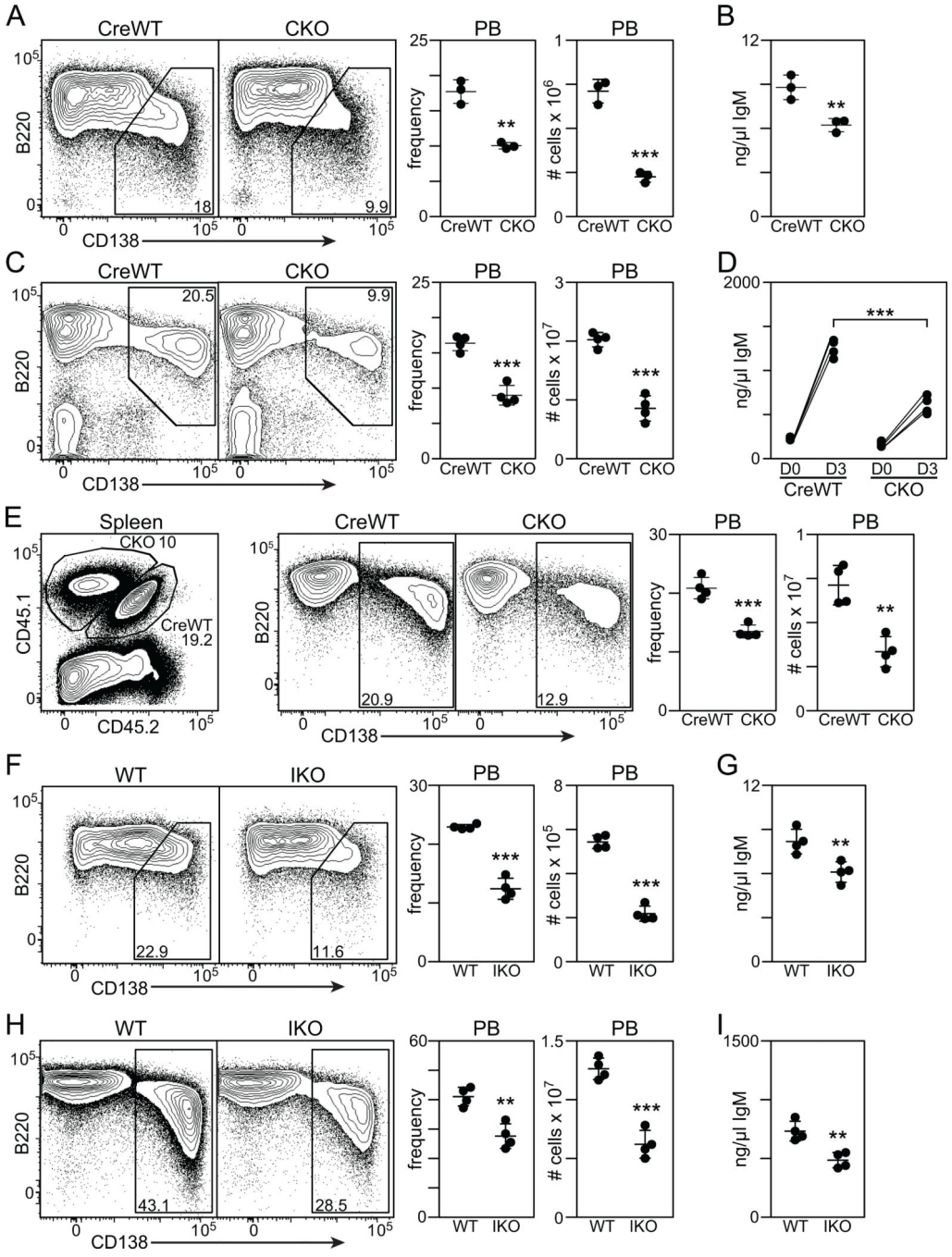

Figure 2 –. LSD1 is required for plasmablast formation.

(A) Flow cytometry analysis of B220 and CD138 expression in *ex vivo* differentiated CreWT and CKO splenic B cells cultures (left) and quantification of $CD138^+$ PB (right). **(B)** IgM media titre of B cell cultures from (A). **(C)** B220 and CD138 expression in CreWT and CKO splenocytes on day three after LPS inoculation (left) and quantification of $CD138^+$ PB (right). **(D)** IgM serum titre of mice from (C) directly before (D0) and on day three after LPS inoculation (D3). **(E)** B220 and CD138 expression in adoptively transferred CreWT and CKO splenocytes on day three after LPS inoculation (left) and quantification of $CD138^+$ PB

(right). **(F)** B220 and CD138 expression in *ex vivo* differentiated WT and IKO splenic B cells cultures (left) and quantification of $CD138^+$ PB (right). **(G)** IgM media titre of B cell cultures from (F). **(H)** B220 and CD138 expression in adoptively transferred WT and IKO splenocytes on day three after LPS inoculation (left) and quantification of $CD138^+$ PB (right). **(I)** IgM serum titre of mice from (H) on day three after LPS inoculation. All data are representative of at least two independent experiments using three to five mice per group. Error bars represent mean ± SD. Significance determined by Student's two-tailed t-test. **P<0.01, ***P<0.001.

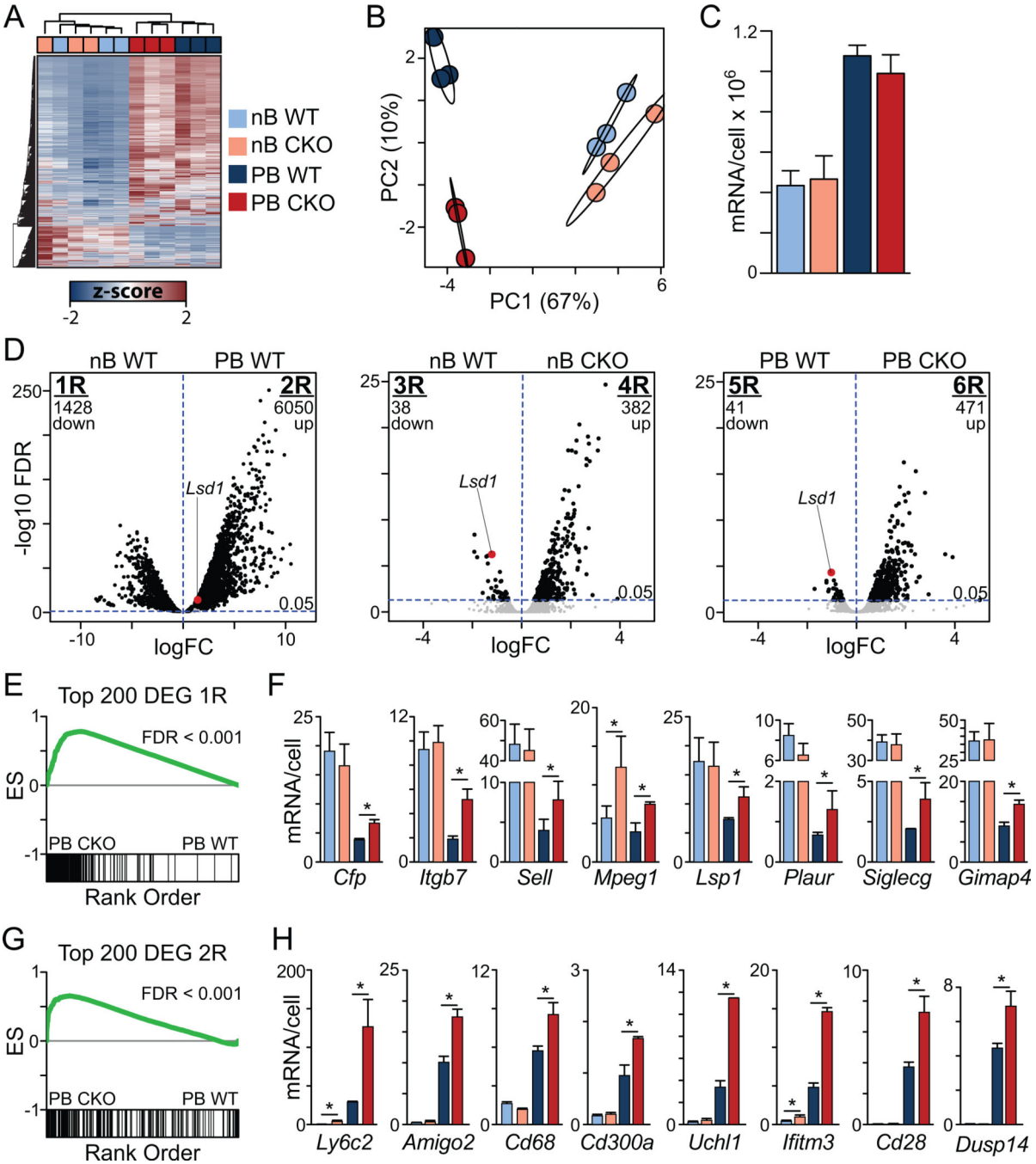

Figure 3 –. LSD1 regulates the plasmablast transcriptional program.

(A) Heatmap of hierarchical clustered, z-score normalized expression data (mRNA/cell) of all 411,909 detected genes between the indicated groups. **(B)** Top two principle components (PC1, PC2) from PCA of z-score normalized mRNA/cell expression of genes from (A). Circles represent 99% confidence intervals. **(C)** Average mRNA per cell per sample group. **(D)** Volcano plots of differentially expressed genes (DEG) between the indicated comparison. Plotted are -log10(FDR) and logFC based off of differential expression analysis of absolute changes in gene expression(9). LSD1 is indicated in each plot (red dot). **(E)**

GSEA analysis of PB WT and PB CKO using a gene set of the top 200 most significant 1R DEG. **(F)** DEG exhibiting derepression in PB. **(G)** GSEA analysis of PB WT and PB CKO using a gene set of the top 200 most significant 2R DEG. **(H)** DEG exhibiting superinduction. Error bars represent mean ± SD. Significance determined by edgeR. **FDR*<0.05.

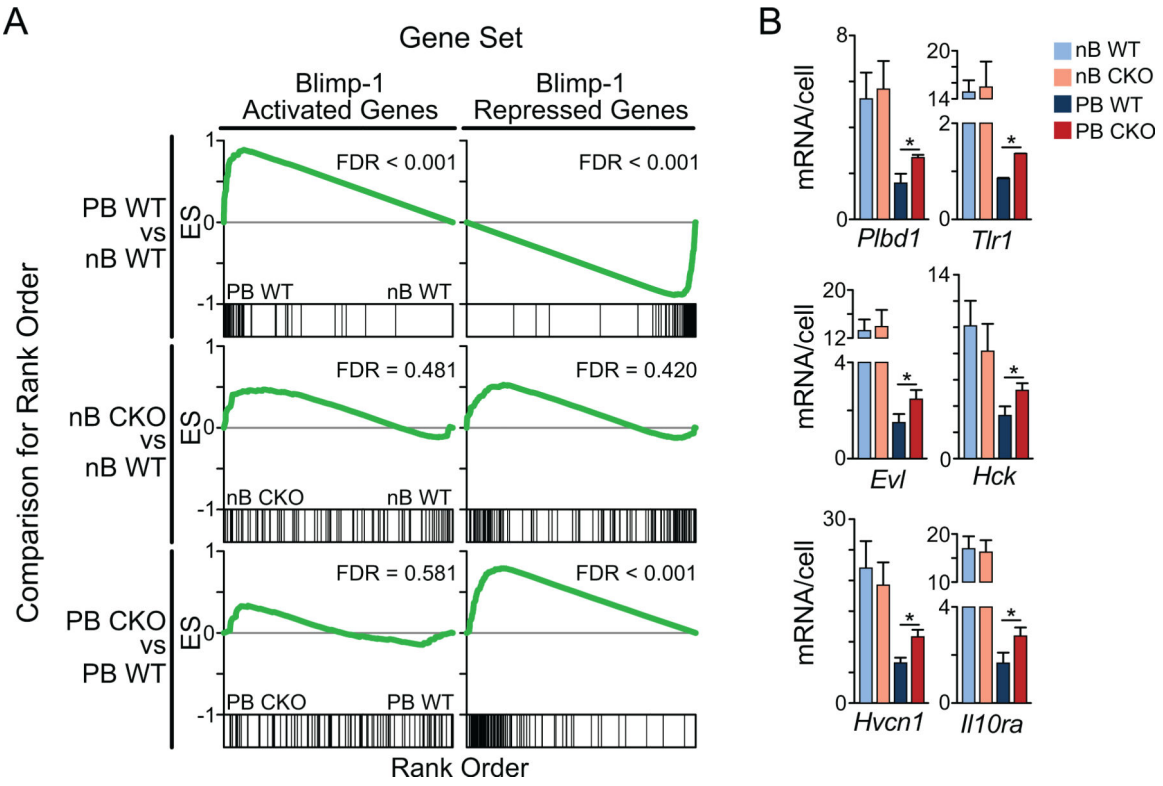

Figure 4 –. Blimp-1 target repressed genes are regulated by LSD1.

(A) GSEA analysis for enrichment of Blimp-1 activated genes (left) and Blimp-1 repressed genes (right)(10) in all detected genes ranked by expression difference between the indicated sample group comparisons. **(B)** Example Blimp-1 target repressed DEG. Error bars represent mean ± SD. Significance determined by edgeR. **FDR*<0.05.

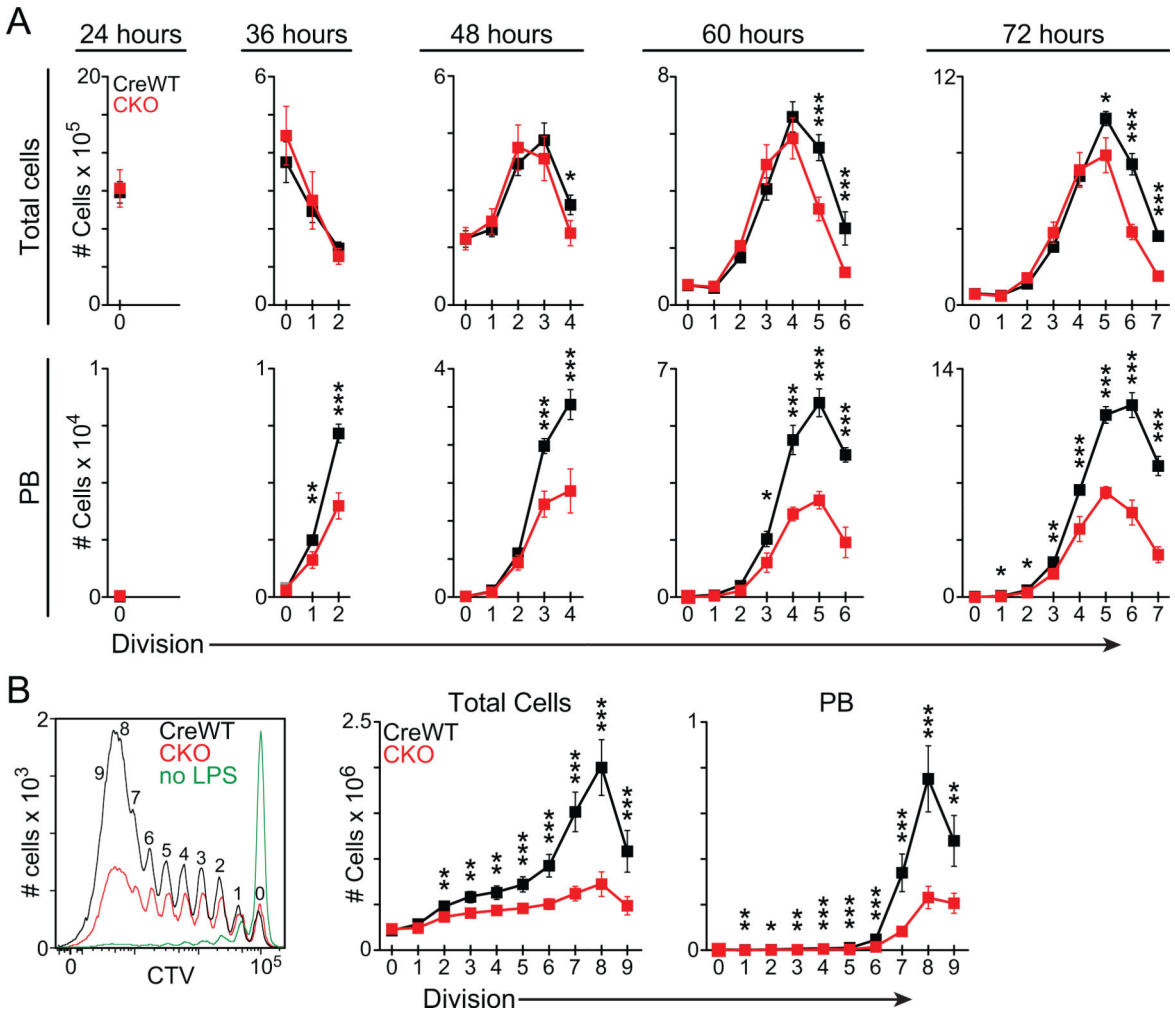

Figure 5 –. LSD1 promotes B cell proliferation.

(A) Flow cytometry analysis of CTV in adoptively transferred CreWT and CKO splenic B cells on day three after LPS inoculation (left) and quantification of total cells and total CD138^{+} PB per division (right). **(B)** Total cells and total CD138^{+} PB per division of *ex vivo* differentiated CreWT and CKO splenic B cells at five time points. Data are representative of at least two independent experiments using three to five mice per group. Error bars represent mean ± SD. Significance determined by Student's two-tailed t-test. **P*<0.05, ***P*<0.01, ****P*<0.001.

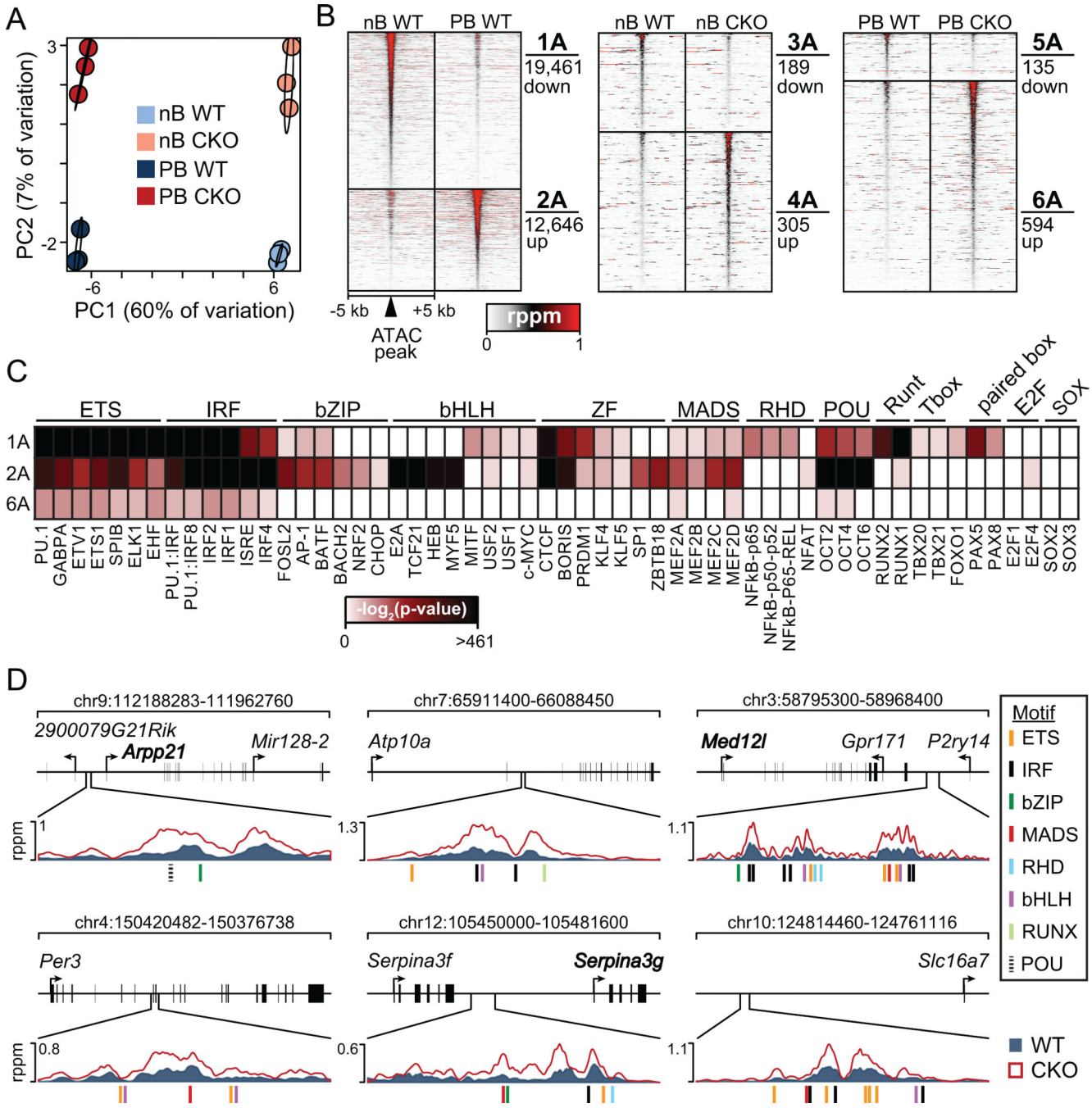

Figure 6 –. LSD1 regulates chromatin accessibility at ETS and IRF transcription factor motifs.

(A) Top two principle components (PC1, PC2) from principle component analysis of z-score normalized rppm values of all ATAC-seq peaks (72,519 total) and sample group 99% confidence intervals (black ovals). rppm, reads per peak per million. **(B)** Heatmap depicting differentially accessible regions between the indicated comparisons. rppm +/− 5 kb around the peak is shown. **(C)** Heatmap displaying -$\log_2$(p-values) for transcription factor binding motifs enriched in the indicated DAR identified through HOMER known motif analysis. **(D)**

Gene tracks of example DAR mapping to a 6R gene. Transcription factor family motifs are indicated by colored dashes under each track.

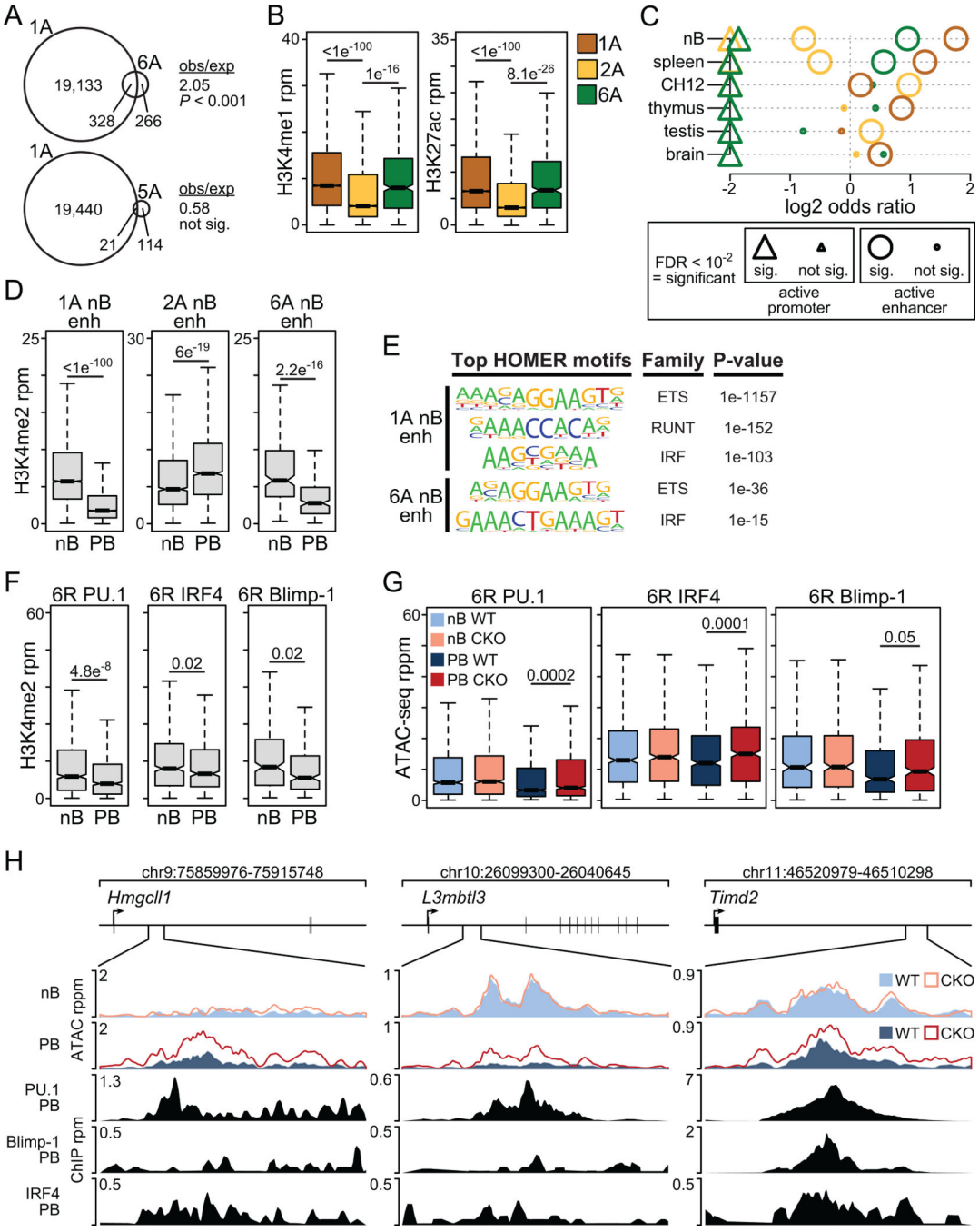

Figure 7 –. LSD1 restricts chromatin accessibility at naïve b cell enhancers in plasmablasts.

(A) Overlap between DAR group comparisons 1A vs 6A and 2A vs 6A. obs/exp refers to the ratio of observed DAR overlap over expected overlap according to a permutation test. **(B)** ChIP-seq rpm enrichment of nB H3K4me1 (left) and H3K27ac (right) for DAR groups 1A, 2A, and 6A. **(C)** Log_2 odds ratios of DAR group enrichment with active enhancers and active promoters from six different cell types. **(D)** Boxplot of ChIP-seq enrichment of nB and PB H3K4me2 for nB enhancers mapping to 1A DAR and 6A DAR. **(E)** Top significantly enriched transcription factor motifs identified through HOMER *de novo* motif

analysis for 1A nB enh and 6A nB enh. **(F)** Boxplot of ChIP-seq enrichment of nB and PB H3K4me2 for PU.1 binding sites, IRF4 binding sites, and Blimp-1 binding sites mapping to 6R DEG. **(G)** Boxplot of chromatin accessibility of the indicated sample groups at 6R PU.1, 6R IRF4, and 6R Blimp-1 regions. **(H)** Gene tracks of example transcription factor binding sites mapping to a 6R gene that exhibit significant increases in chromatin accessibility in PB CKO. Significance determined by Wilcoxon rank sum test (B), Fisher's exact test (C), or Student's two-tailed t-test (D,F,G). rppm, reads per peak per million; rpm, reads per million.

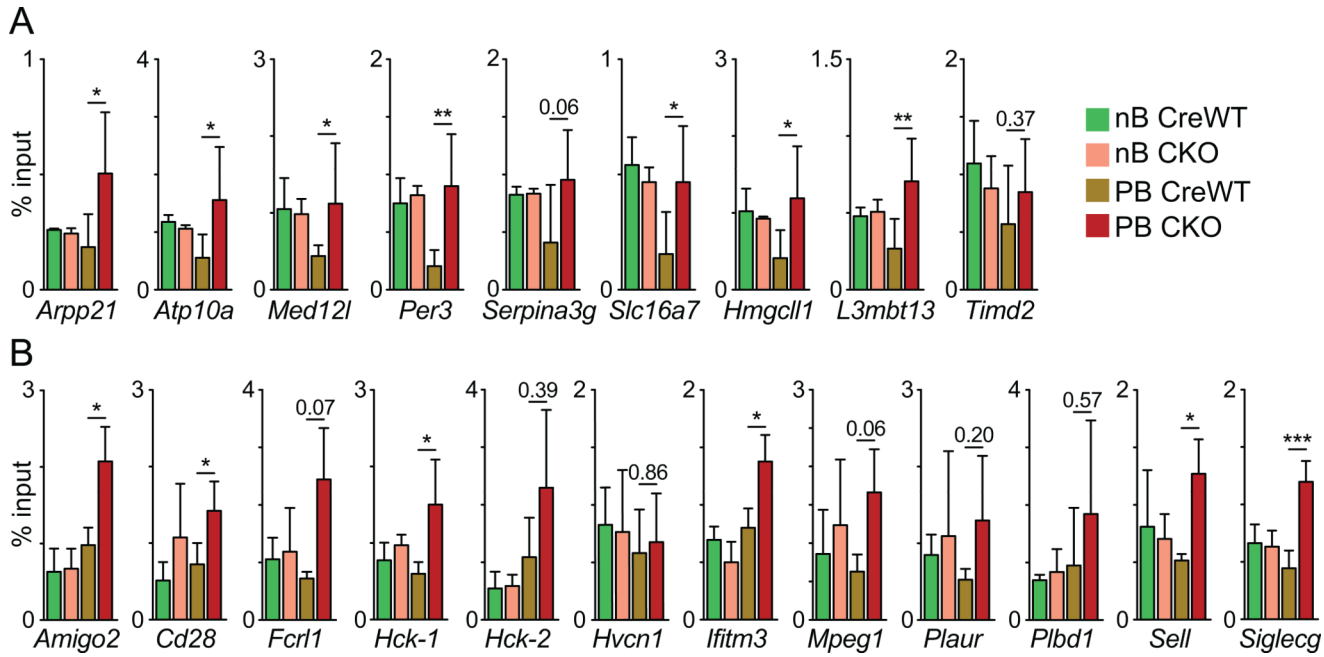

Figure 8 –. Aberrant accumulation of H3K4me1 at LSD1-regulated loci.

(A, B) ChIP-qPCR for H3K4me1 enrichment displayed as % of input at the indicated genomic regions. Data are combined from two independent experiments using three mice per group. Error bars represent mean ± SD. Significance determined by Student's two-tailed t-test. **P*<0.05, ***P*<0.01, ****P*<0.001.